QUANTIFYING BIOAVAILABLE METALS AND POTENTIAL DUST EMISSIONS FROM HIGHWAY-RELATED AND DESERT SEDIMENTS AT LORDSBURG PLAYA, NEW MEXICO

November 2021

Center for Advancing Research in **Transportation Emissions, Energy, and Health**
A USDOT University Transportation Center

Disclaimer

TECHNICAL REPORT DOCUMENTATION PAGE

1. Report No.	2. Government Accession No.	3. Recipient's Catalog No.		
4. Title and Subtitle Quantifying Bioavailable Metals and Potential Dust Emissions from Highway-Related and Desert Sediments at Lordsburg Playa, New Mexico		5. Report Date November 2021		
		6. Performing Organization Code		
7. Author(s) Thomas E. Gill, Iyasu G. Eibedingil, R. Scott Van Pelt, Junran Li, Marcos Mendez, Julieta Saucedo, and Lixin Jin		8. Performing Organization Report No. UTEP-01-13		
9. Performing Organization Name and Address: CARTEEH UTC University of Texas at El Paso, 500 West University Avenue El Paso, TX 79968		10. Work Unit No.		
		11. Contract or Grant No. 69A3551747128		
12. Sponsoring Agency Name and Address Office of the Secretary of Transportation (OST) U.S. Department of Transportation (USDOT)		13. Type of Report and Period Final 01/01/2018–12/31/2020		
		14. Sponsoring Agency Code		

16. Abstract
Lordsburg Playa, a dry lakebed in the Chihuahuan Desert of southwestern New Mexico, is crossed by Interstate 10 (I-10). Clouds of dust blowing from the playa onto the highway represent an acute traffic safety hazard, making I-10 at Lordsburg Playa the deadliest stretch of highway in the United States for dust hazard. Metals contained in Lordsburg Playa dust may represent an additional health risk to motorists and others exposed to them. The research team performed field investigations at Lordsburg Playa to assess land-surface conditions contributing to dust emission, quantify dust emissivity of playa surfaces using a portable in-situ wind erosion laboratory, and collect playa materials for subsequent analysis and modeling. Threshold friction velocities for dust entrainment ranged from < 0.30 ms^{-1} for delta and shoreline areas to > 0.55 m s^{-1} for ephemerally flooded playa areas; mean PM$_{10}$ vertical flux rates ranged from < 500 μg m^{-2}s^{-1} for ephemerally flooded playa areas to ~25,000 m^{-2}s^{-1} for disturbed delta surfaces. The unlimited supply of coarse sediments along the western playa shoreline may contribute particles triggering dust events; this zone should be a focus area for dust mitigation efforts. If playa surface crusts become disturbed, loose sediment underneath is revealed, increasing dust emission potential; thus, activities on the playa that degrade the crust should continue to be restricted. Playa sediments generally were rich in silt, composed of minerals common to regional playas, and contained up to ~20 ppm bioavailable Pb, ~1830 ppm bioavailable Cu, and ~4690 ppm bioavailable Zn (possibly reflecting traffic-related emissions deposited near the highway). Researchers combined two numerical models, the Single-Event Wind Erosion Evaluation Program and the American Meteorological Society and U.S. Environmental Protection Agency Regulatory Model, to estimate the generation and dispersion of dust and PM$_{10}$ from key hotspots during two typical dust event days using data from field and laboratory tests, soil and land databases, and on-playa weather stations. Results from modeling were consistent with observations from traffic webcam photos and visibility records from meteorological sites. The combined models predicted transient dust PM$_{10}$ concentrations of up to ~200,000 μg m^{-3} could impact I-10, presenting acute but short exposures to dust and airborne metals at the highway, although these brief exposures are not likely to significantly impact the long-term aerosol inhalation burden to anyone caught in a playa dust event.

17. Key Words Dust, particulate matter, traffic safety, metals, modeling, New Mexico, desert		18. Distribution Statement No restrictions. This document is available to the public through the CARTEEH UTC website. http://carteeh.org		
19. Security Classif. (of this report) Unclassified	20. Security Classif. (of this page) Unclassified		21. No. of Pages 54	22. Price $0.00

Form DOT F 1700.7 (8-72)   Reproduction of completed page authorized

Executive Summary

Lordsburg Playa in the Chihuahuan Desert of Hidalgo County, New Mexico, is representative of playa (dry lakebed) environments in deserts, which are potent source areas of airborne dust. Lordsburg Playa is crossed by Interstate 10 (I-10), exposing motorists to dense clouds of dust that can suddenly blow across the road and block visibility, creating a severe safety hazard. Despite warning signage on I-10, there have been dozens of traffic fatalities on Lordsburg Playa caused by dust events; frequent closures of the highway when dust is forecast, causing delays in the delivery of goods and services; and congestion and damage on secondary roads used as detours. Lordsburg Playa has already become a priority site for environmental remediation to reduce dust emission to improve highway safety and reduce detour-related delays and losses. In addition to metals from historic mining activity that may have been deposited on Lordsburg Playa, traffic-related metals from vehicular emissions may also have settled on the playa near the highway; if resuspended by wind in dust storms, these metals could create not only a traffic safety hazard but also a health hazard to motorists and highway and public safety workers on I-10.

The research team performed field studies at Lordsburg Playa to investigate its geomorphology and land-surface characteristics, identify likely focus areas of dust emission and the processes that may be facilitating wind erosion, sample dust-emitting sediments for further analysis, and measure the physical properties of the playa and surrounding environments. Researchers used a Portable In-Situ Wind ERosion Laboratory (PI-SWERL) to field-test dust and PM_{10} particulate matter (a federally regulated air pollutant) emissivities of different Lordsburg Playa environments representing different landscape positions, sediment and soil characteristics, land management, and disturbance histories. Sediment samples were analyzed in the laboratory for mineralogy (via X-ray diffraction), grain size distribution (via laser diffraction), and bioavailable metals (via inductively coupled plasma mass spectrometry of silt fractions leached in simulated lung fluids). Researchers combined two numerical models, the U.S. Department of Agriculture's Single-Event Wind Erosion Evaluation Program (SWEEP) and the American Meteorological Society and U.S. Environmental Protection Agency Regulatory Model (AERMOD), to simulate and predict soil loss and dust emissions from playa hotspots and estimate PM_{10} concentrations that could be experienced at I-10.

Field observations and analyses made it apparent that the actual lakebed surface is not strongly dust emissive when intact and undisturbed. However, shoreline margins or beach areas and delta areas where sediments from the surrounding basin are brought into the playa are highly dust emissive and should be the focus areas of management to mitigate wind erosion and dust emission, including limiting disturbance and reestablishing and augmenting sediment-trapping, native vegetation where feasible. The field tests with the PI-SWERL showed a wide range of values for threshold friction velocity, friction velocity at which the National Ambient Air Quality Standard would be exceeded in a 30-m column of air (representing formation of a dust cloud), PM_{10} vertical flux rates, and total PM_{10} vertical flux during the tests—reflecting the complexity and variability of surfaces on Lordsburg Playa and its surroundings. The critical friction velocities and dust emissivities were most dependent on surface crust strength, thickness, and disturbance and less dependent on the surface sediment texture. Thus, processes that disturb the playa surface enough to break or remove surface crusts from the large, indurated region of the playa will increase the dust emissivity. The western shoreline of the playa was the most emissive of the sites tested and was one of the few areas without dust supply limitation even though the surface sediments contain by far the lowest percentage of PM_{10}, which is likely due in part to legacy sediment control structures (dams and berms) on the east slopes of the Peloncillo Mountains above the playa that release pulses of sediment onto the western playa surface. For these reasons, this area should be a priority for dust emission control measures followed by delta areas that appear to develop more fragile crusts.

Chemical and mineralogical analysis showed that playa sediments at different landscape positions consistently contained calcite, quartz, feldspars (plagioclase and potassium feldspar), analcime, and illite/mica. Some samples

also contained trace amounts of chlorite, other carbonate minerals, and zeolites. All of these minerals are expected constituents of playa environments in the southwestern United States. Simulated lung fluid leachates of playa sediments contained up to approximately 20 ppm of lead (near the highway), more than 4000 ppm of zinc (near the highway), and more than 1800 ppm of copper (far from the highway). Grain size analysis of Lordsburg Playa sediments revealed many sites with extremely high silt, clay, and inherent PM_{10} contents, suggesting very high potential wind erodibility.

This study was the first to successfully combine the SWEEP wind erosion model and the AERMOD air dispersion model to evaluate PM_{10} dispersion in a playa environment. The modeling was informed by the field and laboratory data from the samples collected from Lordsburg Playa, federal soil and land use/land cover databases, and weather data from meteorological stations on the playa and other regional sites. Based on the outputs from the SWEEP model, the AERMOD model characterized the spatiotemporal dispersion of PM_{10} at 6800 receptors across the playa. Dust plumes originating on the playa, including dust clouds from large, highly emissive areas of the playa away from the highway as well as smaller, less emissive playa fields located directly upwind of the interstate, can lead to PM_{10} exposures at the highway at the hourly scale of tens to hundreds of thousands of micrograms per cubic meter. Since the highest concentrations of lead were found nearest to the highway, dust events could result in high short-term exposures to airborne lead (also a federally regulated air pollutant). Acute exposures to airborne zinc and potentially other metals, which have been shown in other studies to be associated with human health effects, may also occur at I-10 during dust events. However, since these particulate exposures will be brief, their human health effects may not be severe and may be less of a concern than the traffic safety hazard. The combination of a wind erosion model with a particulate dispersion model could be adopted during site selection for effective assessment of wind-transported fugitive dust at other playas and dust hotspots that threaten transportation corridors and other infrastructure.

Lordsburg Playa has been closed by the U.S. Bureau of Land Management to off-highway vehicle use since 1998 to reduce soil disturbance that leads to wind erosion. However, unauthorized, crust-destroying activities still take place on the playa surface, so the playa should be carefully monitored for and protected against activities that disturb the crust and increase dust emissions. In order to improve highway safety and reduce the risk of continued visibility-related crashes and shutdowns, rigorous monitoring and enforcement of these protections should be encouraged. Even a small area of disturbed playa in the wrong place and an unfortunate gust of wind could initiate a dust plume crossing the highway, dangerously reducing visibility, increasing exposure to extremely high concentrations of PM_{10} and its constituents including metals, and creating a health and safety hazard to traffic on I-10. By identifying the most emissive dust sources and estimating the magnitudes of dust exposure that would be experienced at the roadside, priority areas can be identified that could reduce the visibility and dust exposure hazard along this section of I-10 and make it no longer the dust-deadliest stretch of highway in the United States.

Extensive projects for remediation of the dust hazard, coordinated by the New Mexico Department of Transportation and other agencies, are underway. This project has contributed to the knowledge base and scientific underpinning of these efforts to resolve the dust exposure and highway safety problem where I-10 crosses Lordsburg Playa. The project contributed to the education and research training of an undergraduate student, master's student, and doctoral degree recipient at the University of Texas at El Paso. A doctoral dissertation resulting from this study has been completed, two open-access peer-reviewed scientific papers have been published, and 20 presentations have been given at scientific conferences and workshops; this report is extracted in part from them. More publications and presentations are in the works.

Acknowledgments

Table of Contents

List of Figures

List of Tables

Background and Introduction

According to the World Health Organization (2018), traffic crashes are the ninth leading cause of death worldwide. In the United States, on average, the annual death toll from motor vehicle crashes due to weather-related visibility and vision hazards such as fog, smoke, dust, and blowing sand exceeds the number of fatalities caused by other weather-related hazards including tornadoes, floods, tropical cyclones, and lightning (Ashley et al., 2015; Bhattachan et al., 2019). Due to the arid climate of the deserts of the southwestern United States, fog, the most common weather phenomenon affecting highway visibility nationwide (Ashley et al., 2015), is rare along highway corridors in desert regions of the Southwest.

Anthropogenic materials are emitted into and settle onto the surrounding environment from vehicles traveling on highways. These anthropogenic materials include tailpipe emissions from fuel combustion, as well as particles from the wear of tires, brakes, and other engine parts. Although lead was completely phased out in motor vehicle fuels in the United States decades ago, its legacy may remain in roadside sediments (Kayhanian, 2012). Brake-derived non-exhaust particulates are enriched in a wide variety of metals and settle on and near roads (Grigoratos and Martini, 2015), and the wear of rubber tires releases zinc into the environment (Councell et al., 2004), accumulating in roadside soils (Smolders and Degryse, 2002). All of these metals and others pose a potential human health concern when ingested or inhaled (Morman and Plumlee, 2013; Adamiec, 2017), especially when associated with airborne dust (the silt and clay size fraction of sediments, < 50 µm), which is also prone to contain higher concentrations of metals (Al-Rajhi et al., 1996) than coarser particles.

Windblown (aeolian) dust and sand crossing transportation corridors in drylands is increasingly recognized as a direct threat to human health and safety in itself (Baddock et al., 2013; Goudie, 2014; Middleton, 2017; Li et al., 2018; Zheng-chao, 2018; Bhattachan et al., 2019; Davari et al., 2019). Dust and sand blowing across roadways causes sudden loss of visibility (Ashley et al., 2015) (Figure 1) and reduced traction on the road surface (Davari et al., 2019; Pan et al., 2021), and together they increase the likelihood for loss of vehicle control and collisions. Goudie (2014) searched newspaper clippings for 12 consecutive months in the period of 2012 to 2013 and reported that dust-related fatal highway crashes happened in six U.S. states in a single year. Numerous case reports have been published on blowing and drifting dust and sand causing highway crashes, especially multi-vehicle incidents on high-speed roads including interstate highways (Pauley et al., 1996; Laity, 2003; Goudie, 2014; Deetz et al., 2016; Nicoll et al., 2020). The U.S. National Weather Service (NWS) reported that dust events are the third largest weather-related cause of highway casualties in the state of Arizona, resulting in at least 157 fatalities and 1324 injuries statewide in 50 years (Lader et al., 2016).

Note: Photo courtesy of David Dubois.

Figure 1. Thick dust blowing across Interstate Highway 10 in New Mexico.

Dust and sand blowing across highways not only constitutes a direct health and safety hazard but also causes significant economic impacts. A single traffic fatality was estimated to cost the United States $1.38 million in 2010 when medical care, emergency services, productivity over a lifetime, insurance, workplace costs, and legal costs were considered (Blincoe et al., 2015). Beyond healthcare-related costs from crashes, aeolian dust and sand crossing highways disrupts and delays transportation and delivery of goods, services, and people; increases costs for deployment of highway maintenance and public safety personnel; and causes significant property damage. Dust and sand crossing highways is a significant "off-site" cost of wind erosion (Pimentel et al., 1995; Baddock et al., 2013). In 2005, the Federal Highway Administration (FHWA) noted that commercial shippers and carriers valued transit time at $25 to $200 per hour, depending on the value and perishability of the product being carried, so weather-related delays or detours on major transportation corridors caused by dust storms also cause significant economic losses as well as health and safety hazards. Only a few studies have provided an in-depth analysis on the occurrence of such events, and little information is available to highway managers on the mitigation and management of this hazard (Li et al., 2018).

Semiarid and arid regions of the world are disproportionate sources of windblown sand (Pye and Tsoar, 2009) and dust aerosols (Prospero et al., 2002; Zobeck and Van Pelt, 2006). Playas (dry or intermittently wetted lakebeds in internal drainage basins), being flat, windswept, and unvegetated, are prominent source areas of dust storms globally (Prospero et al., 2002) including the Chihuahuan Desert of southwest North America (Baddock et al., 2011a, 2011b). Hard-crusted surfaces typically forming the inner part of the playa (Gillette et al., 2001) and fluctuations in sediment loading and supply at the edge of the playa (Lee et al., 2009) are critical controlling factors modulating dust emission on playas. A fully hard-crusted surface without loose soil particles on top of it significantly reduces dust emissions (Gillette et al., 2001). However, these types of surfaces can evolve to become continuous sources of dust when the interparticle bonds of the crust are broken—for example, by anthropogenic activities including disturbance by motor vehicles or livestock—and when the surface is supplied with sediments from its surrounding basins through runoff (Houser and Nickling, 2001; Macpherson et al., 2008). Moreover, the development of dust storms and wind-induced disturbances can create a positive feedback degrading the crust strength, leading to the development of thin and soft crusts that are erodible by the wind (Cahill et al., 1996; McKenna Neuman et al., 2005; McKenna Neuman and Maxwell, 2002). Comparing soil crusts, Langston and McKenna Neuman (2005) showed that salt crusts break down and erode sooner than biological crusts to wind disturbances as the strength of a crust varies with the composition and spatial distribution of the binding media.

Playas act as receptacles accumulating the materials eroded from the surrounding watersheds. When the surrounding uplands include metal deposits, especially if unearthed and released through mining and the exposure of mine wastes, the metals can accumulate in the wind-erodible surface sediments of the playa (Reheis et al., 2002). The principal investigator's works (Gill, 1995; Gill et al., 2002) and those of others (Kim et al., 2014) show that metal-enriched sediments from playas and mining-impacted sites yield metal-enriched dusts.

In addition to irritation and inflammation caused by inhalation of particulate matter of any composition, additional human health effects may result from inhalation or ingestion of potentially toxic substances contained within or coating the particles. Metal-bearing mineral dusts, for example, those associated with mining activity, are known to pose specific human health risks that may vary with their mineral composition and/or metal concentrations (reviewed by Fubini and Arean, 1999). While in-vitro metal availability has been widely explored for the gastrointestinal system, for which the U.S. Environmental Protection Agency (EPA) and European Union have protocols (Drexler and Brattin, 2007; Wragg, 2011), fewer methods are available for exploring respiratory availability (Wiseman, 2014; Wiseman, 2015) due to the complexity of the respiratory system's composition and pH variations, and because ingestion had been recognized as the main exposure pathway for metals (Martin et al., 2018). Wiseman (2015) evaluated simulated lung fluids (SLFs) as a method of leaching metals from particulate matter or soil samples for assessment of potential respiratory toxicity and identified different major variables in a leaching protocol that controls the release of metals, including the elemental chemistry and pH of SLF, particle size of the sediments used, sediment-to-SLF solution ratios, temperature, and duration of the leaching experiment.

Numerical models of wind erosion can play a significant role in characterizing soil loss and dust emission from aeolian transport hotspots, such as agricultural fields, industrial sites, or, as in this study, a playa. One model widely used for such purposes is the U.S. Department of Agriculture's (USDA's) Wind Erosion Prediction System (WEPS) (Tatarko et al., 2016). The WEPS erosion submodel, the Single-Event Wind Erosion Evaluation Program (SWEEP), is appropriate to use to model dust emission from nonagricultural disturbed lands if estimates are available on surface soil/biomass conditions and meteorological parameters (USDA Agricultural Research Service [USDS-ARS], 2007; Tatarko et al., 2016). The model calculations in SWEEP are identical to the WEPS erosion model but are independent of the five other submodels that build the WEPS model (Tatarko et al., 2016). The erosion submodel initiates the process by determining static threshold friction velocity at which erosion begins for each cell based on the surface conditions including random and oriented roughness; flat biomass, crust, and rock cover; cover of loose, erodible aggregates on the crust; aggregate size distribution; density of uncrusted surface; and surface wetness (Hagen et al., 1995). Following that, the soil loss is determined any time the friction velocity exceeds the static threshold friction velocity.

The SWEEP model predicts potential soil loss from single-day windstorm events using site-specific surface soil/biomass conditions and meteorological parameters in terms of total soil loss (particle size < 2.0 mm), creep/saltation (0.1 to 2.0 mm), suspension (< 0.1 mm), and PM_{10} (< 0.01 mm) flux entering the atmosphere (Hagen et al., 1995; Tatarko et al., 2016). The estimated potential PM_{10} emission output from the SWEEP model can then be used as a primary input to an air dispersion model used to examine the temporal and spatial exposures to the public health and safety from particulate matter pollution. Although the SWEEP model has been widely used in estimating soil loss from agricultural lands, fewer studies have tested this model for nonagricultural land uses (Maurer and Gerke, 2011; Jia et al., 2014; Pi et al., 2016; Tatarko et al., 2016). For example, Maurer and Gerke (2011) and Jia et al. (2014) employed the SWEEP model to simulate aeolian sediment fluxes from an artificial hydrological watershed and a tailings dam, respectively, where both have conceptually similar settings as that of a desert playa.

Air dispersion models employ mathematical formulations to characterize atmospheric dispersion, chemical, and physical processes of pollutants emitted by a source over space and time (Holmes and Morawska, 2006; U.S. EPA, 2010). The American Meteorological Society and EPA Regulatory Model (AERMOD), one of EPA's preferred and

recommended air quality dispersion models, is a steady-state plume model that incorporates airborne pollutant dispersion based on planetary boundary layer turbulence structure and scaling concepts providing estimates of ambient concentrations (U.S. EPA, 2019). As an output, the model provides estimates of ambient pollutant concentrations primarily for regulatory purposes (Cimorelli et al., 1998; Heckel and Lemasters, 2011). AERMOD aims at simulating near-field (< 50 km) dispersion from a variety of polluting sources and model configurations including rural and urban settings, surface and elevated sources, fixed and mobile sources, and simple and complex topographical settings (Zou et al., 2010; Rood, 2014; U.S. EPA, 2019). Among other dispersion models, AERMOD has been extensively applied to simulate PM_{10} pollutant dispersion from different source types including transportation emissions (Chavez and Li, 2020), industrial sites (Amer and Abbas, 2015; Hadlocon et al., 2015; Fadavi et al., 2016), agricultural fields (Botlaguduru, 2010), mining areas (Tartakovsky et al., 2016; Tian et al., 2019), and landfill sites (Westbrook and Sullivan, 2006; Chalvatzaki et al., 2015). Focusing on the dust-emissive playa of Mono Lake, California, Ono et al. (2011) assimilated sand flux monitoring, ambient PM_{10} monitoring, and the AERMOD model to estimate dust emissions and their downwind impact on a receptor site, confirming the superiority of the AERMOD model in these types of topographical settings as compared to other air dispersion models.

Site Description

This investigation focused on and took place at Lordsburg Playa in Hidalgo County, in the northwestern Chihuahuan Desert of southwestern New Mexico, just east of the Arizona state line. The location of Lordsburg Playa in southwestern North America is shown in Figure 2. Lordsburg Playa is not only one of the sources of the most intense dust storms in the Chihuahuan Desert (Rivera et al., 2010) but is also crossed by Interstate 10 (I-10) (Figure 3), the southernmost transcontinental highway in the U.S. Interstate Highway System, and a major transportation artery extending from Florida to California. Approximately 15,000 vehicles per day, about 30 percent of which were trucks, crossed the playa on I-10 in 2016 (Haas, 2017). The Union Pacific railroad crosses Lordsburg Playa parallel to and generally approximately 30 m north of the interstate.

Lordsburg Playa is the only dust-emitting playa crossed by an interstate highway in the southwestern United States, although ~1000 km north of Lordsburg, Interstate Highway 80 crosses the playa of Great Salt Lake, Utah, and has been the location of fatal dust-related traffic wrecks (Nicoll et al., 2020). Plumes of airborne dust and sand crossing I-10 close to their source on the Lordsburg Playa (Figure 4) therefore represent an immediate safety hazard to roadway motor vehicle traffic due to sudden loss of visibility and resulting driver disorientation (Ashley et al., 2015; Li et al., 2018). According to Botkin and Hutchinson (2020), at least 120 dust events affected the Lordsburg Playa during the eight years from 2012 to early 2020.
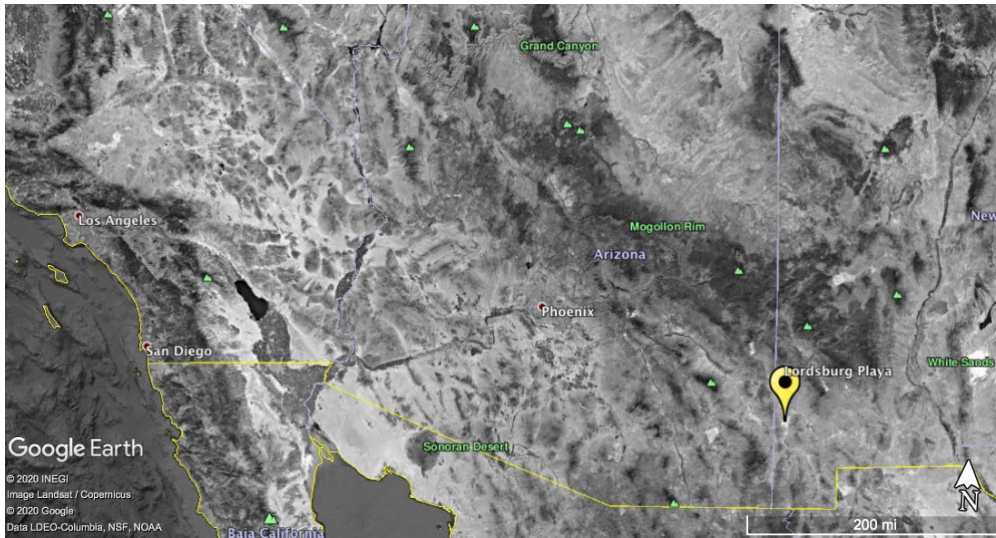
Figure 2. Location of Lordsburg Playa in southwestern North America.
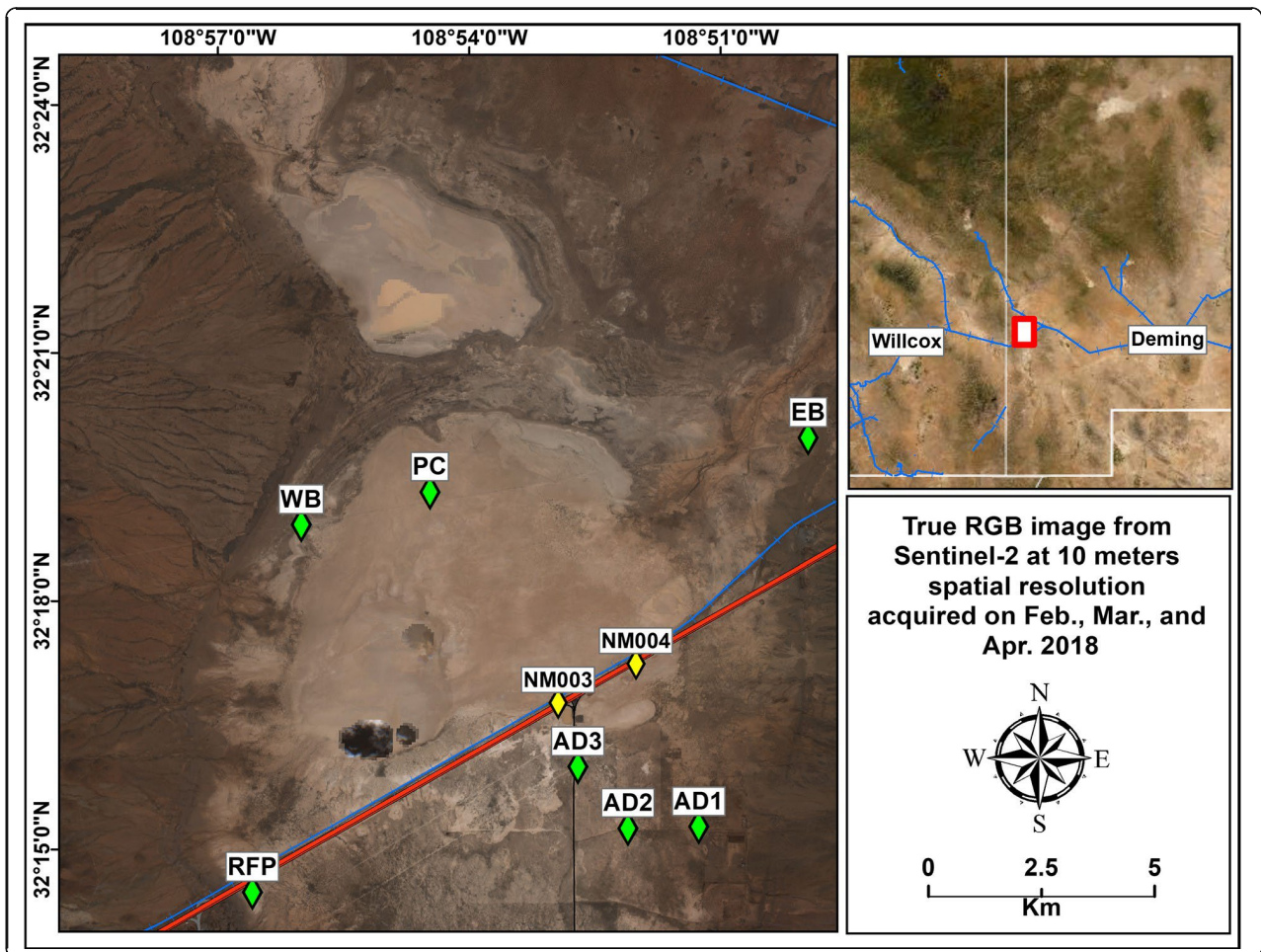
Note: This figure shows the locations (green diamonds) of the surfaces that were tested in the field with the PI-SWERL as listed in Table 2 and the New Mexico Department of Transportation weather stations (NM003 and NM004) (yellow diamonds).

Figure 3. Satellite image of Lordsburg Playa dissected by I-10 (red) and Union Pacific Railroad (blue).

Note: Photo by Thomas Gill.

Figure 4. I-10 crossing Lordsburg Playa, looking east, with plumes of airborne sand and dust crossing the highway advecting from north to south in the central part of the playa, March 22, 2016.

Lordsburg Playa comprises several intermittently connected, ephemerally flooded, otherwise-dry lakebeds in the northern part of the Animas Basin within the basin and range physiographic province and the northwestern Chihuahuan Desert ecoregion. These dry lakebeds represent the bottom of Pleistocene Lake Animas (Allen and Lucas, 2005). The lakes are the termination of drainage from the Pyramid Mountains, the south and west slopes of Burro Peak, the eastern slopes of the Peloncillo Mountains, and the west and north slopes of the Animas Mountains. The largest and southernmost of the dry lakebeds is sometimes named Kathrine Playa (PC), and is the lakebed traversed by I-10. The altitude of the lakebed is approximately 1263 m above mean sea level, and the climate is arid, with approximately 30 cm of average annual precipitation, more than half of which typically falls during the North American monsoon between late June and September. Five months of the year have average maximum temperatures in excess of 30°C, with June, the hottest month, having an average maximum of 35°C. Rainstorms during the summer monsoon can cause the typically dry playa to become at least partially inundated with standing water and wet overall (Eibedingil et al., 2021). These summer floods and flows from the surrounding uplands load soil and sediments, potentially acting to enhance dust emission, onto the playa through fluvial transport. Additional pulses of sediment are released onto the playa from breaching of unmaintained historic tanks and berms in the surrounding highlands, especially the east slopes of the Peloncillo Mountains (Botkin and Hutchinson, 2020).

The playa develops crusts on its surfaces once the water evaporates, the outflow rate being greater than the inflow rate. Lordsburg Playa has been closed by the U.S. Bureau of Land Management (BLM) to off-highway vehicle use since 1998 "to reduce impacts to the soil on the Lordsburg Playa. Once the soil surface is disturbed, it is highly susceptible to wind erosion" (U.S. Department of the Interior, Bureau of Land Management, 1998). Anthropogenic disturbances to the playa that disrupt the crust (livestock and vehicular traffic) have been suggested to alter the surface hydrology, degrade vegetation, and expose loose erodible sediment and saline-sodic soils; these disturbances facilitate the generation of dust storms on the Lordsburg Playa complex (Klose et al., 2019; Van Pelt et al., 2020; New Mexico Department of Transportation, 2020). Observations of the authors and New Mexico state employees suggest that unauthorized, crust-destroying activities still take place on the playa surface.

The drainages of the Lordsburg Playa watershed have long been known to be rich metal mining prospects (Laskey, 1938), with a legacy of multiple mines active in the first part of the twentieth century extracting over 1.5 million tons of silver, copper, gold, zinc, manganese, iron, and lead ores (Laskey, 1938; McLemore and Elston, 2000). These ores were also assayed to contain enhanced concentrations of other metals including > 1000 ppm arsenic and hundreds of parts per million antimony (McLemore and Elston, 2000). The ultimate settling basin of the weathering products of these ores, as well as waste products of these mining enterprises, is the playa. Thus, sediments of Lordsburg Playa itself might contain enriched concentrations of metals that may be released in the dust, irrespective of any additional contributions of metals or other contaminants from highway emissions that settled onto the soil close to I-10.

Soils in the Lordsburg Playa Basin are classified primarily as Aridisols of the Hondale series (Fine, mixed, superactive, Thermic Natargid) in the Animas Creek delta and along the western shoreline; Playas series (Fine, mixed, superactive, Sodic Haplocambid) in the ephemerally flooded lakebed; and small areas of Vertisols of the Verhalen silty clay loam series (Fine, smectitic, thermic Typic Haplotorrerts) on the eastern shoreline. Although the playa surface is saline and alkaline with occasional salt efflorescences (puffy growths of evaporite minerals on the surface) (Reynolds et al., 2007), the surface sediments have been described as being comprised of primary silicate and clay minerals with lower concentrations of evaporites (salt minerals) than many other dust-emitting playas in North America (Hibbs et al., 2000; Mitroo et al., 2019). Vegetation of the area is typical of the lower elevation Chihuahuan Desert, with dominant shrubs including saltbush (*Atriplex* spp.) and seablight (*Suaeda nigrescens* I.M. Johnst), with alkali sacaton (*Sporobolus airoides* (Torr.) Torr.) as the dominant grass in the saline areas and sand dropseed (*Sporobolus cryptandrus* (Torr.) Gray) and ring muhly (*Muhlenbergia torreyi* (Kunth) Hitchc.) in well-drained, sandier areas above the shoreline. Following closure of the mining districts in the Lordsburg Basin during the early twentieth century, livestock grazing is the primary land use in the surrounding area.

Problem

I-10 across Lordsburg Playa has been recently judged to have the greatest dust hazard of any stretch of highway in the United States (Tong et al., 2021). Despite extensive fixed highway signage on and approaching the playa in both directions (Figure 5), at least 117 dust-/wind-related traffic crashes were recorded on I-10 crossing Lordsburg Playa by public safety authorities between 1980 and 2017 (New Mexico Department of Transportation, 2018). At least 41 dust-related traffic fatalities have occurred since 1965 (Figure 6), including 21 deaths since 2012 and seven persons killed in one dust event in May 2014 and 10 killed in four dust events during 2017 (Associated Press, 2017; Botkin and Hutchinson, 2020).

Note: Photo by Scott Van Pelt.

Figure 5. Highway signs warning of dust hazard and prescribing safe actions for drivers in reduced visibility as vehicles approach Lordsburg Playa on I-10.

Note: Photo by Scott Van Pelt.

Figure 6. Memorial to victims of a dust-related traffic crash on the south side of the I-10 right of way on Lordsburg Playa.

I-10 across Lordsburg Playa was closed to traffic for dust-related safety reasons at least 39 times between 2012 and 2019 (Botkin and Hutchinson, 2020). When the highway is closed, vehicles must either wait, potentially for hours, until weather conditions abate or detour 172 km and an additional > 2 h travel time onto two-lane secondary roads not designed for heavy truck traffic (Arizona Department of Transportation [ADOT], 2019), causing economic losses not only from increased travel time and other logistical delays but also as a result of damaging pavement and bridges on the structurally weaker alternate routes. To facilitate the detour's increased traffic flow during high wind events and make this route safer, ADOT planned to spend nearly $60 million (ADOT, 2019). The New Mexico Department of Transportation (NMDOT) has spent approximately $2 million in recent years (Trent Botkin, NMDOT, personal communication) to assess and mitigate the dust threat. Meanwhile, other agencies, including FHWA, BLM, and the USDA Natural Resources Conservation Service (NRCS), as well as contractors have joined with both states' departments of transportation, working diligently together to attempt to mitigate this hazard with engineering-based and biological (vegetation-based) dust control approaches.

In addition to the hazard of injury and economic disruption from closures and crashes, there is a risk of exposure to extremely high concentrations of airborne particulate matter in the form of mineral dust and its constituents including metals (derived from mining-enriched playa sediments, or near-roadside sediments contaminated by emissions from highway traffic) for anyone in the vicinity of Lordsburg Playa during a wind event. Those exposed could include motorists crossing the playa on the highway or stopped during a dust storm or safety closure. Public safety personnel, railway workers, state and county highway/roads department and state transportation department employees, researchers, natural resource managers, landowners, grazing leaseholders, and other persons who may find themselves on or adjacent to the Lordsburg Playa are also at risk from inhalation of dust during wind events in the Lordsburg Basin.

This Center for Advancing Research in Transportation Emissions, Energy, and Health (CARTEEH) project leveraged the team's previous expertise in assessment of near-highway dust exposures (Li et al., 2017, 2018) and stakeholders' efforts. The aim was to home in on assessing the causes and drivers of Lordsburg Playa dust exposures by quantifying actual dust emissions from likely source areas, evaluating the levels of bioavailable metals in wind-erodible sediments on Lordsburg Playa, and modeling dust and PM_{10} emission intensity from playa hotspots and subsequent exposures at I-10. None of these tasks had been previously undertaken with regard to Lordsburg Playa. With this knowledge, land managers—both public and private—in partnership with transportation and public safety authorities may be able to prioritize areas for control to mitigate future dust

outbreaks, as well as understand the potential level of dust and PM_{10} exposure along the highway, thus protecting human health and safety and reducing economic impacts of blowing dust and sand.

Approach

This project included field, laboratory, and numerical modeling activities. The research team performed this investigation to assess the physical and chemical properties and dust emissivities of likely potential dust source materials surrounding and within Lordsburg Playa; assess the potential toxicity and bioavailability of dust-producing sediments on the playa surface; and with those data, model the potential particulate matter exposures along I-10 using a wind erosion model (SWEEP), with its outputs serving as some of the inputs for a dispersion model (AERMOD).

To accomplish these objectives, the researchers used widely accepted instrumentation and methodologies to directly measure the physical and chemical characteristics, bioavailable metal concentrations, in-situ-generated dust emissions, and erodibility for many representative surfaces at Lordsburg Playa under a range of conditions. With these data, the research team used the coupled models to simulate the soil loss, saltation/creep (large particle) loss, suspension (dust) transport, and PM_{10} emissions from selected portions of the playa under windy, dusty conditions. The team characterized the spatiotemporal dispersion of the PM_{10} emissions from the playa at the receptor site (transportation corridor) to represent the potential dust exposure at the highway.

Methodology

Field and Laboratory Data Collection

Between 2018 and 2020, project personnel made numerous field reconnaissance visits to Lordsburg Playa and the surrounding basin to observe playa surface and environmental conditions under a variety of weather conditions, collect samples of sediments and soils to be returned to the laboratory for chemical and physical analysis, and perform various field-based measurements related to wind erosion and dust emission. Sediment/soil samples were collected following USDA soil sampling protocols with plastic tools (retired after each sample was collected) (Figure 7) and stored in sealed plastic bags or containers at the Department of Geological Sciences at the University of Texas at El Paso (UTEP) to avoid the possibility of metal contamination.

Note: Photo by Iyasu Eibedingil.

Figure 7. Collecting sample of sediment surface crust at Lordsburg Playa using plastic tools and containers.

The particle size distribution (PSD) of all surface soil samples collected from field visits to the Lordsburg Playa Basin was measured by laser diffraction spectroscopy at the Arid Environments Laboratory of the principal investigator at the UTEP Department of Geological Sciences, generally following the procedures of Sperazza et al. (2004). Soil

samples were passed through a 2-mm sieve to remove any gravel or plant debris, and 0.2 to 0.6 g of the sieved sample was dispersed in 11.5 ml of a sodium hexametaphosphate solution. The 15-ml tubes containing the dispersed sample were shaken in a reciprocating shaker for at least 8 h before introduction to the Malvern Mastersizer 2000 (Malvern Instruments, Worcestershire, UK) that had been calibrated using 0.2 g of ISO 12103-1 A4 coarse test dust. For each dispersed sample, three individual PSD determinations were made, and the means of each PSD class were calculated. From these means, the researchers determined the percentage of sand ($53 < d < 2000$ μm), silt ($2 < d < 53$ μm), clay ($d < 2$ μm), and PM_{10} ($d < 10$ μm) in each of the soil samples.

Mineralogical characterization was performed at the U.S. Geological Survey in Reston, Virginia. To prepare sediments for mineralogical characterization, samples were hand ground using an agate mortar and pestle and sieved to 40-mesh. Samples were packed into 32-mm side-loaded aluminum sample holders. X-ray diffraction (XRD) analysis was performed using a PANalytical X'Pert PRO (Almelo, Netherlands) automated powder diffractometer with a 15-mm mask operating at Cu Kα radiation at 45 kV and 40 mA. Samples were rotated at 8 RPM during the analysis, while the angle was scanned from 3 to 80 °2θ at a step size of 0.0167° with a counting time of 60 s per point. Quantitative mineral phase identification was performed using the Reitveld module of PANalytical X'Pert HighScore Plus software (Almelo, Netherlands; version 4.5.0.22741) and standard reference patterns from the Inorganic Crystal Structure Database (Fiz Karlsruhe, 2013). Reitveld refinements were performed using a Chebyshev background correction; unit cell parameters were allowed to vary.

The analysis of bioavailable metal concentrations in wind-erodible Lordsburg Playa sediments was conducted in the laboratory of Dr. Lixin Jin at the UTEP Department of Geological Sciences. Soil samples were sieved with non-metallic sieves with mesh diameter < 63 μm to focus on silt-sized particles that would form the suspension mode and could potentially be inhaled in a wind event. An amount of 100 mg ± 0.3 mg was weighed and placed into a 50-ml centrifuge tube. An SLF solution was created using the method of Davies and Feddah (2003), Julien et al. (2011), and Martin et al. (2018), which is considered to best represent human lung conditions. The SLF solution was prepared mixing the compounds in Table 1 in order under constant stirring. Dipalmitoylphosphatidylcholine (DPPC), the final component, represents the surfactants existing in the alveoli; DPPC was prepared separately and added slowly to the solution under constant stirring. 50 ml of the SLF solution was added to the sediment sample to keep a ratio of 1:500 between solid sample and solution. The mixture was vigorously shaken by hand, sealed, and kept in an incubator for 2 h at a temperature of 37.0 ± 0.5°C, and then removed and centrifuged for 2 min at 18,000 G. The supernatant was decanted for analysis without filtration into clean 15-ml centrifuge tubes, acidified using HNO_3, and stored at 4°C until elemental analysis with inductively coupled plasma mass spectrometry (ICP-MS). Fresh 50 ml of SLF was added to the centrifuge tubes, and the procedure was repeated for 4-, 6-, and 24-h incubation times. The solutions were diluted with 5 percent nitric acid to lower the ionic strength and analyzed for Cu, Pb, and Zn concentrations via ICP-MS, along with procedure blanks, calibration standards, and check standards.

Table 1. Chemicals and Their Concentrations (in mg/L) in the Simulated Lung Fluid

NaCl	$CaCl_2 \cdot 2H_2O$	Na_2HPO_4	$NaHCO_3$	Trisodium citrate $\cdot 2H_2O$	NH_4Cl	Glycine	DPPC
6400	255	150	2700	160	118	190	0.02%

In the field, the research team conducted tests of surface dust emissivity at Lordsburg Playa using a Portable In-Situ Wind ERosion Laboratory (PI-SWERL) (Etyemezian et al., 2007). The PI-SWERL (Figure 8) is a computer-controlled aspirated cylindrical chamber approximately 30 cm in diameter that entrains dust by rotating a metallic ring a few centimeters above the soil surface, creating the shear stress necessary to entrain loose particles. The cylindrical chamber is aspirated with 1.67 ls^{-1} of filtered air, and a portion of the exhaust is continuously drawn into a DustTrak, a fast response nephelometer (Model 8530, TSI Instruments, Shoreview, Minnesota), to measure PM_{10} concentrations. The PI-SWERL has been shown to provide data on dust emissions and surface erodibilities very similar to a larger linear wind tunnel (Sweeney et al., 2008) and has proven useful for estimating dust

emissivities at other playas including Salton Sea, California (King et al., 2011); Yellow Lake, Texas (Sweeney et al., 2016); and several playa surfaces in Namibia (Von Holdt et al., 2019). For tests on the Lordsburg Playa surfaces, the researchers set the PI-SWERL on a surface typical of the surrounding area (Figure 8) and initiated a 9-min (540-s) hybrid test (Table 2). The hybrid PI-SWERL test intervals and RPMs had been previously determined in preliminary tests on a wide variety of soil surfaces throughout the United States to provide consistency for comparisons among various studies and locations. The hybrid test uses a combination of both ramps and steps during a single measurement. The hybrid test was chosen over a continuous RPM ramp because it identifies surfaces that are not supply limited. Similar hybrid tests have been used for previous studies (Kavouras et al., 2009; Etyemezian et al., 2014; Fick et al., 2019). Following test initiation, the PI-SWERL was controlled by and all test data, including data from the DustTrak, were logged in an imbedded computer. Test operation data were monitored in real time, and the test discontinued protecting the optical bench of the DustTrak if the PM_{10} concentration exceeded 400,000 $\mu g/m^3$.

Table 2. Summary of the Hybrid PI-SWERL Testing Used to Assess Surface Dust Emissivities and Threshold Friction Velocities at Lordsburg Playa

Cumulative Test Time (s)	Interval Time (s)	Operation
0–540	540	Aspirate PI-SWERL bell and record PM_{10} concentration
0–60	60	No ring movement
61–105	45	Accelerate ring to 2000 RPM
106–165	60	Maintain ring at 2000 RPM
166–210	45	Accelerate ring to 3000 RPM
211–270	60	Maintain ring at 3000 RPM
271–315	45	Accelerate ring to 4000 RPM
316–375	60	Maintain ring at 4000 RPM
376–420	45	Accelerate ring to 5000 RPM
421–480	60	Maintain ring at 5000 RPM
481–540	60	Decelerate ring to 0 RPM

Note: Photo by Scott Van Pelt.

Figure 8. PI-SWERL in test configuration on Lordsburg Playa undisturbed surface with polygonal crusts.

Seven sites in the Lordsburg Playa Basin (shown in Figure 3) were tested with the PI-SWERL, with at least four replications conducted on fresh surfaces at each of the sites. Three of the sites were located on delta deposits on the fringe of the playa associated with Animas Creek south of I-10 and represented land used for cattle grazing designated as sites AD1, AD2, and AD3. Two of the sites had thick, hard, clay-rich lacustrine sediments that dried into indurated crusts with distinct polygons (as can be seen in Figure 7, Figure 8, and Figure 9[d]), designated sites RFP and PC. Finally, two of the sites were shoreline (beach) areas at the eastern and western margins of the lakebed, designated as sites EB and WB, respectively. At each replicated test location, global positioning system (GPS) coordinates were recorded, approximately 100 g of the 0–5 cm surface sediment was sampled, and the surface threshold friction velocity ($u*_t$) was estimated using the airgun and penetrometer technique of Li et al. (2010). Where both undisturbed and disturbed (cattle tracks or vehicle tire tracks) surfaces were sampled for a total of 44 tests, GPS coordinates and soil samples were obtained. Estimates of $u*_t$ using the airgun and penetrometer technique were terminated after 37 tests due to instrument malfunction. Analysis of collected airgun and penetrometer data revealed that this method may not provide reliable results on playa soils due possibly to the presence of soluble salts.

From PI-SWERL data, friction velocities, $u*$ (a measure of shear-related motion in moving fluids that may result in vertical entrainment of particles) were obtained at a frequency of 1 Hz by regressing the rotating ring RPM versus Irwin sensor-measured friction velocity data provided in the PI-SWERL Operator Manual v1.3 Fig. 1.2 (Dust-Quant, 2011) and entering the instantaneous rotating ring RPM into the resulting regression equation. PI-SWERL estimates of threshold friction velocity $u*_t$ (the friction velocity at which particles will become entrained in the fluid) were not simple; the researchers almost always saw an initial spike in PM_{10} concentration both when the airflow started during the first few seconds of the test and again at the first few seconds of rotating ring acceleration to 2000 RPM. This spike phenomenon is possibly due to vibration within the PI-SWERL at startup dislodging particles within the system. Under both these test phases, the researchers saw the PM_{10} concentrations fall to near pretest levels within 30 s after the initial spike. The research team visually determined the $u*_t$ by

inspecting the PM_{10} concentration curve to determine when the fresh PM_{10} was being entrained from the ground surface. PM_{10} emissivity expressed as mass per unit time per unit area was calculated by dividing the instrument-determined vertical flux rate data ($\mu g\ s^{-1}$) by the 0.026 m^2 effective area of the rotating ring.

The 2-m mean wind velocity that would result in an exceedance of the U.S. EPA National Ambient Air Quality Standard (NAAQS) for PM_{10} of 150 $\mu g\ m^{-3}$—representing the minimum visibility-reducing dust cloud—was calculated by taking the measured PM_{10} concentration in the PI-SWERL that would result in a 30-m mixed column of air with PM_{10} that would equal or exceed the PM_{10} NAAQS. The height of the inside of the bell of the PI-SWERL is 20 cm. The 30-m height for mixing was arbitrarily chosen because it is quite possible in turbulence for PM_{10} to mix to this height. Thus, by multiplying the NAAQS standard by 150 times the inside depth of the bell from which dust measurements were obtained, the concentration inside the bell must be at least 22.5 mg m^{-3} for this value to be reached or exceeded. The friction velocity calculated for this 1-s time step was subsequently entered into Prandtl's equation using 0.4 for von Karman's Constant and a mean value from several sources of 2×10^{-5} m for the roughness length of a bare smooth surface to obtain the expected mean wind speed at 2 m. Wind speed is nearly universally reported at the standard reported height of 2 m, which would be the mean reported wind speed at which the PM_{10} NAAQS would be exceeded over similar surfaces. The same calculation based on Prandtl's equation was used to estimate the threshold wind speed for PM_{10} entrainment. These wind speeds are based on a smoother bare surface as tested by the PI-SWERL, and due to vegetation surrounding the bare surfaces that were tested, the actual threshold wind speeds would probably be greater than the values fit.

Weather data were collected from two NMDOT weather stations located along I-10 on the lakebed, NM003 and NM004 (shown in Figure 3). The stations were established on July 22, 2015, and record 15-min wind speed means and maximum gust. These data, an average of 35,064 observations per year, were compared to the estimated threshold wind speeds for PM_{10} entrainment, exceedance of the U.S. EPA NAAQS, and the wind speed at which the maximum dust entrainment was observed during the PI-SWERL to estimate the percentage of observations exceeding these values. The last date of data considered was July 1, 2020.

Statistical analysis of the PI-SWERL and associated data was done using Proc GLM in SAS v9.4. Means were separated using Ryan's Q. Regression relationships between the response parameters and surface factors including soil texture and percent PM_{10} were performed in Microsoft Excel graphs by fitting trendlines, linear equations, and R^2 values for the relationships.

Numerical Modeling

SWEEP
The SWEEP model simulation was run for two areas of the playa (fields) (Figure 9) identified as potentially emitting dust that could impact I-10 for two dust event days. One field was along the southern edge of North Playa, located to the north of I-10 and Union Pacific Railroad, a region identified as a frequent source of dust plumes blowing south across I-10 (seen in Figure 4). The other field was Road Forks Playa (RFP), an ephemerally flooded small playa south of the highway where I-10 enters the Lordsburg Basin from the west; this area has been the site of frequent dust plumes propagating northward, and a focus for BLM and NMDOT mitigation efforts (U.S. Department of Interior, Bureau of Land Management, 2018; NMDOT, personal communication). The dust event days selected were February 3, 2020, and June 5, 2020, representing spring and summer and synoptic-scale and convective (thunderstorm outflow) driven events, respectively, typical of the two seasons and meteorological drivers of the vast majority of dust events in the Chihuahuan Desert (Novlan et al., 2007). These days were selected through analysis of visibility data from the NM003 and NM004 meteorological sites and webcam photos from NMDOT traffic cameras.
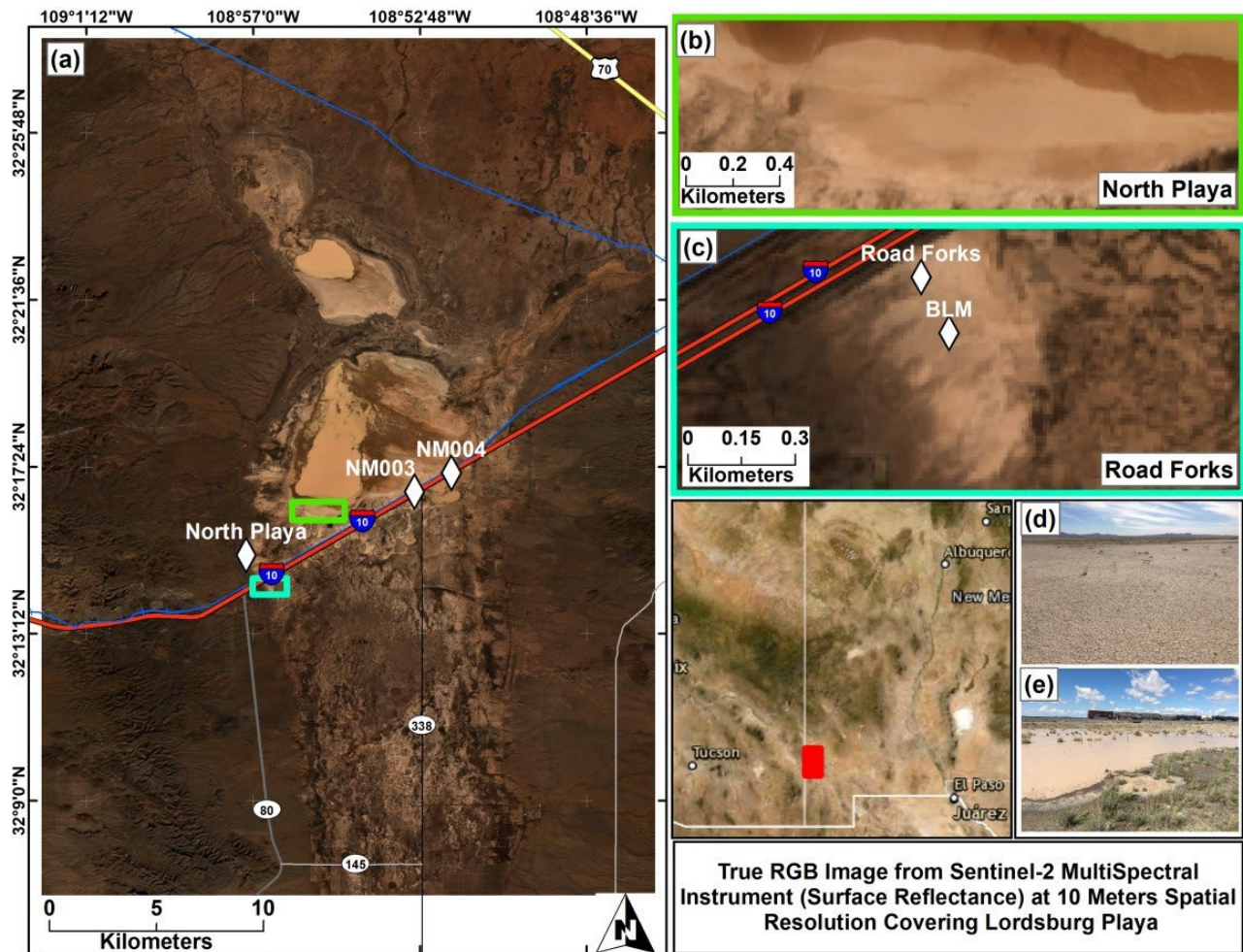
Notes:

(a) True RGB (Band 4—Red, Band 3—Green, and Band 2—Blue) image of the study area covering Lordsburg Playa from Sentinel-2 MSI (MultiSpectral Instrument) Level 2A at 10-m spatial resolution (Gascon et al., 2017). The North Playa field is bounded by the green rectangle, and the RFP field is bounded by the blue-green rectangle.

(b) North Playa field used to simulate soil loss using SWEEP model.

(c) Road Forks field used to simulate soil loss using SWEEP model.

(d) Example of hard-crusted surface from the inner part of the playa on March 7, 2018.

(e) Inundated area on playa just south of highway and railroad on September 20, 2018.

Figure 9. True RGB image from Sentinel-2 MSI (surface reflectance) at 10-m spatial resolution covering Lordsburg Playa.

The SWEEP model was primarily designed to characterize soil loss from rectangular fields only. To address this limitation, the irregular-shaped fields at Lordsburg Playa were divided into strips of rectangular subfields. For the February 3, 2020, event, the field from North Playa was divided into 12 rectangular subfields and the field from Road Forks into nine rectangular subfields, covering 3.171 km^2 and 0.279 km^2, respectively (Figure 10 and Table 3). In all four cases, the rectangular-shaped subfields were aligned with the wind direction obtained from the NMDOT meteorological stations (Figure 3). For North Playa field, rectangles were aligned at 232.69° and 124.44° from true north on February 3 and June 5, 2020, respectively. For Road Forks field, the rectangles were aligned at 251.19° and 161.58° from true north on February 3 and June 5, 2020, respectively. For both dates combined, 39 SWEEP model simulations were performed for the 39 subfields. These runs represented the worst-case scenario of maximum possible wind erodibility of the surface.
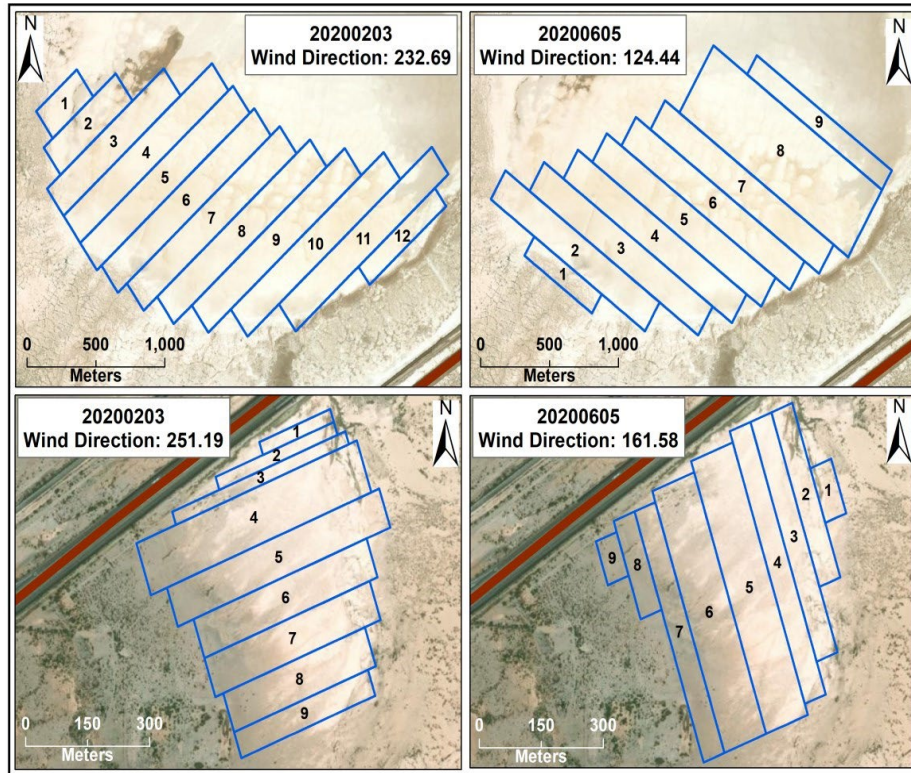
Note: This geometry was used by SWEEP and AERMOD models to simulate soil loss and dust and PM$_{10}$ dispersion, respectively, during dust events of February 3, 2020, and June 5, 2020.

Figure 10. Geometry of field locations at North Playa (top) and Road Forks (bottom).

Table 3. X-Length and Y-Length Input Parameters Used for Simulating Soil Loss at Lordsburg Playa in the SWEEP Model (Length in Meters and Area in m^2)

Field	Date											
	February 3, 2020						June 5, 2020					
	North Playa			Road Forks			North Playa			Road Forks		
	x	y	Area	x	y	Area	x	y	Area	x	y	Area
1	213.13	401.70	85604	29.62	186.02	5509	143.25	619.88	88785	54.30	125.04	6789
2	213.14	714.72	152188	29.62	309.80	9182	214.90	1416.86	304400	54.30	400.11	21724
3	213.15	1159.38	247308	29.62	454.74	13467	214.90	1549.33	332938	54.30	550.15	29871
4	213.16	1472.94	313893	118.48	579.22	68561	214.90	1549.69	332935	54.31	625.17	33944
5	213.17	1517.59	323410	88.86	558.08	49585	214.90	1549.68	332932	108.61	625.17	67889
6	213.17	1517.61	323415	88.86	454.67	40403	214.90	1549.67	332929	108.61	600.17	65174
7	213.17	1517.62	323419	88.86	434.07	38567	214.90	1549.65	332925	54.31	575.16	31229
8	213.17	1517.63	323421	88.86	372.07	33057	501.39	1549.66	776808	54.30	225.06	12220
9	213.17	1517.63	323423	59.24	351.57	20814	143.27	1239.69	177553	54.30	100.03	5431
10	213.17	1517.64	323424	—	—	—	—	—	—	—	—	—
11	213.17	1517.64	323424	—	—	—	—	—	—	—	—	—
12	142.10	757.98	107808	—	—	—	—	—	—	—	—	—

Note: — means not applicable.

As required by the SWEEP model, 38 parameters were defined through the model's series of tabs: field, biomass, soil layers, soil surface, and weather (Table 4). These groups define vegetation and residue characteristics, soil properties, and weather characteristics. The majority of the soil layer and soil properties' data were acquired from

the Soil Survey Geographic (SSURGO) database (Soil Survey Staff NRCS USDA, 2019) by creating areas of interest from the imported shapefiles of North Playa and Road Forks fields. The biomass associated data were extracted from BLM data collected in accordance with the assessment, inventory, and monitoring strategy (Bobo et al., 2018). Meteorological parameters (wind speed, wind direction, and air temperature) were retrieved from the NMDOT meteorological stations NM003 and NM004 accessed through the New Mexico Climate Center. Daily time series of wind speed and air temperature for the four cases used in the study are given in Figure 11. The average daily air temperature and elevation of the fields were used to estimate air density for the day. Hourly wind speeds were used to run the erosion simulation, fulfilling the requirement of the AERMOD model for hourly pollutant emission. Hourly surface water content required by the soil surface tab was assumed to be zero to consider the worst-case scenario. Soil PSD (volumetric particle size) analyses were based on results of the laser diffraction analyses of soil samples collected during field visits. Plots of the cumulative volume percentage versus particle size (0.01 to 2000 µm) from the laser diffraction analyses were used to illustrate the PSDs. In addition, these data were used to extract fractions of sand, very fine sand, silt, and clay using d < 0.002 mm for clay, 0.002 mm < d < 0.05 mm for silt, 0.05 mm < d < 0.1 mm for fine sand, and 0.1 mm < d < 2 mm for sand as particle size categories recommended by the SWEEP model user guide (USDA-ARS, 2007). The textural composition of soil samples representing the North Playa field (Figure 12) was silt loam, while soil at the Road Forks site (Figure 13) had a loam texture. These observations were also supported by the USDA SSURGO database.

Table 4. Parameters Required by the SWEEP Model to Simulate Wind Erosion for the Two Selected Plots

Parameters	North Playa		Road Forks		Source of Data
	20200203	20200605	20200203	20200605	
1. Field					
x and y of fields	Refer to Table 3				
Angle	52.69	304.44	71.19	341.58	Wind direction via New Mexico Climate Center
Number of fields	12	9	9	9	—
Wind barriers	0	0	0	0	—
2. Biomass					
Residue average height (m)	0	0	0	0	BLM
Residue stem area index (m²/m²)	0	0	0	0	
Residue leaf area index (m²/m²)	0	0	0	0	
Residue flat cover (m²/m²)	0	0	0	0	
Growing crop average height (m)	0	0	0	0	
Growing crop stem area index	0	0	0	0	
Growing crop leaf area index	0	0	0	0	
Row spacing (m)	0	0	0	0	
Seed placement	Furrow	Furrow	Furrow	Furrow	
3. Soil Layers					
Number of layers	2		3		NRCS, USDA
Thickness	150, 1370		200, 330, 990		
Sand fraction (Mg/Mg)	0.18, 0.031		0.18, 0.311, 0.551		Soil sampling and PSD analysis from field visits
Very fine sand fraction (Mg/Mg)	0.13, 0.024		0.13, 0.086, 0.111		
Silt fraction (Mg/Mg)	0.59, 0.444		0.59, 0.309, 0.174		
Clay fraction (Mg/Mg)	0.1, 0.525		0.1, 0.38, 0.275		
Rock volume fraction (m³/m³)	0, 0		0, 0, 0		NRCS USDA through SSURGO database
Dry bulk density (Mg/m³)	1.491, 1.491		1.307, 1.677, 1.426		
Avg. aggregate density (Mg/m³)	1.8, 1.8		1.8, 1.8, 1.8		
Avg. dry aggregate stability (ln(J/kg))	2.73, 2.73		3.018, 3.359, 3.348		
GMD of aggregate sizes (mm)	4.914, 26.174		4.409, 11.118, 17.7		
GSD of aggregate sizes (mm/mm)	14.989, 10.506		14.745, 14.735, 12.778		
Minimum aggregate size (mm)	0.01, 0.01		0.01, 0.01, 0.01		
Maximum aggregate size (mm)	36.8, 59.748		36.042, 44.489, 51.383		
Soil wilting point w. content	0.267, 0.267		0.103, 0.217, 0.145		
4. Soil Surface					
Surface crust fraction (m²/m²)	0.5		0.5		Klose et al. (2019)
Surface crust thickness (mm)	10		10		Field visits
Loose material on crust (m²/m²)	0.8		0.8		Klose et al. (2019)
Loose mass on crust (kg/m²)	1.5		1.5		Assumed
Crust density (Mg/m³)	1.8		1.8		NRCS USDA through SSURGO database
Crust stability (ln(J/kg))	2.73		3.02		
Allmaras random roughness (mm)	4		4		
Ridge height (mm)	0		0		
Ridge spacing (mm)	10		10		
Ridge width (mm)	10		10		
Ridge orientation (deg)	0		0		
Dike spacing (mm)	0		0		
Snow depth (mm)	0		0		
Hourly surface water content	0		0		Assumed
5. Weather					
Air density (kg/m³)	1.0692	0.9993	1.0698	0.9999	Estimated
Wind direction (deg. from north)	232	124.44	251.19	161.58	New Mexico Climate Center
Anemometer height (m)	10	10	10	10	
Aerodynamic roughness (mm)	25	25	25	25	NRCS, USDA
Z_0 location flag	Station	Station	Field	Field	New Mexico Climate Center
Number of interval/day to run	24	24	24	24	
Wind speed (m/s)	Refer to Figure 11				

Note: — means not applicable.
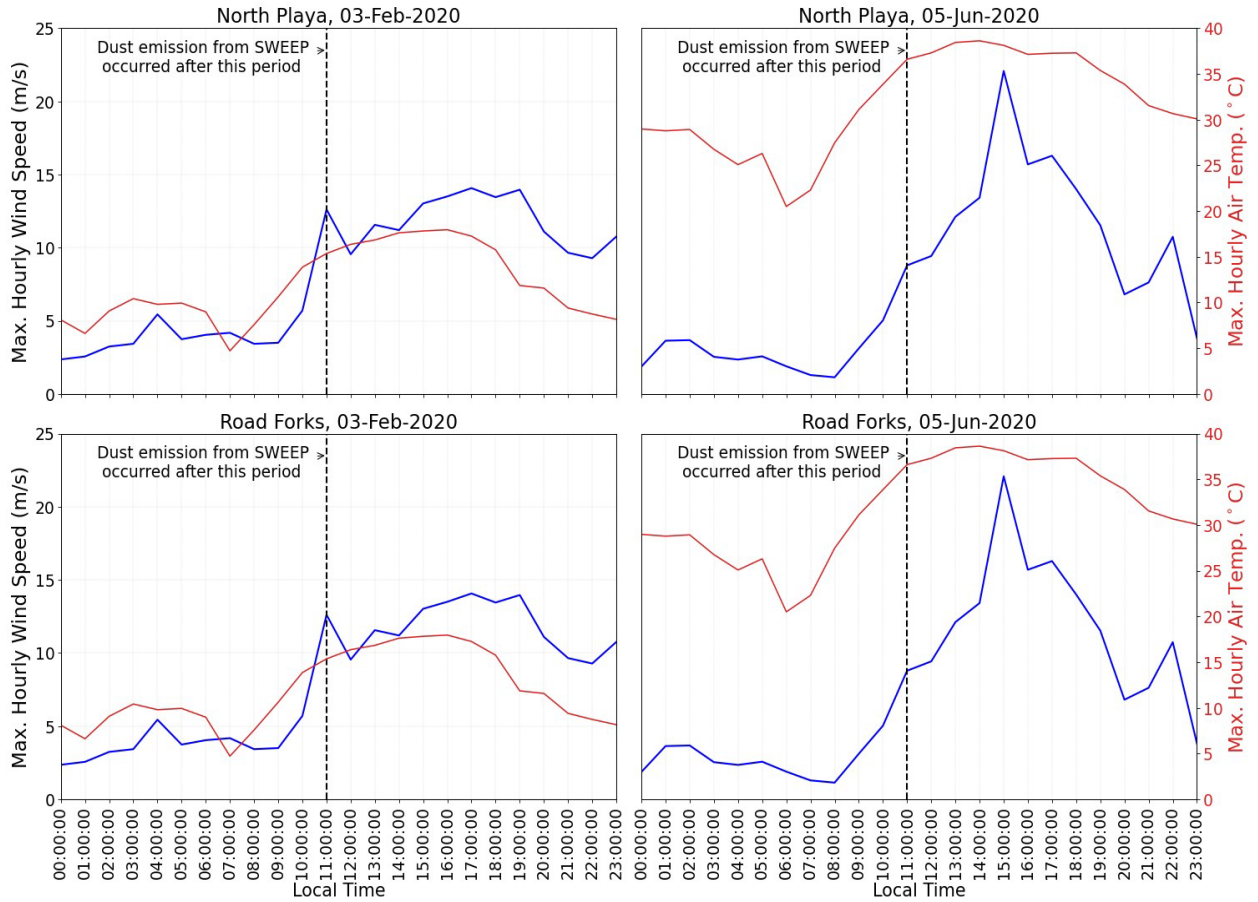
Figure 11. Meteorological data of wind speed and air temperature required by SWEEP for the two sites and cases.
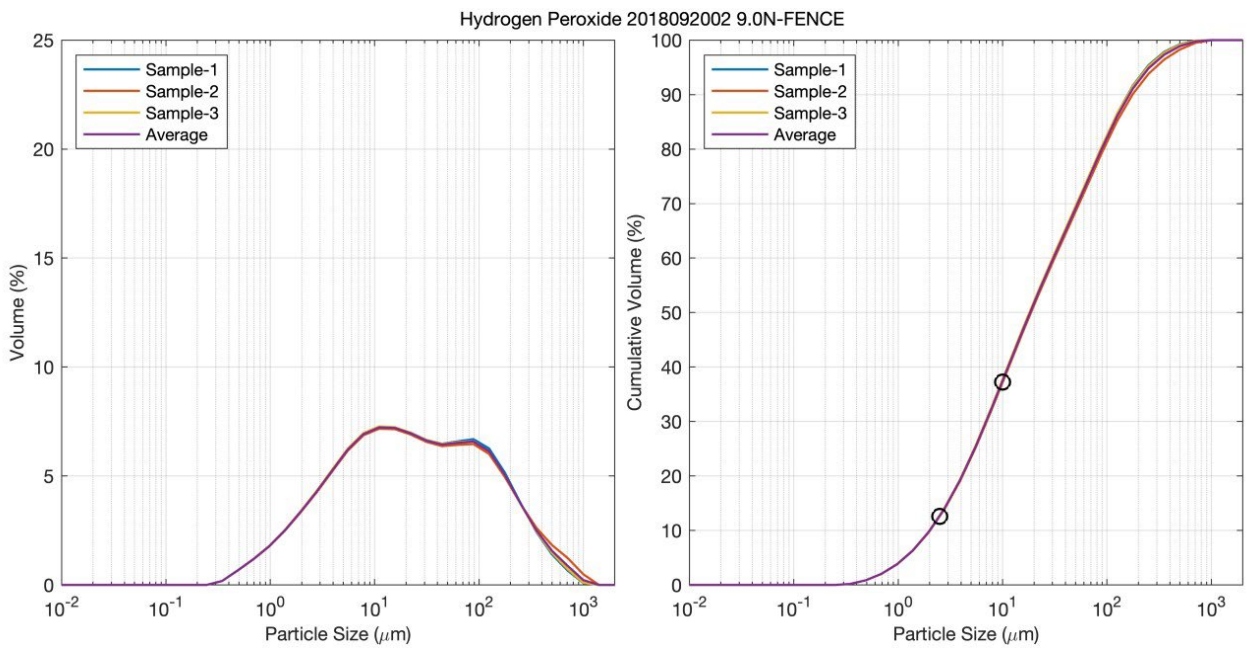
Figure 12. Grain size distribution of the soil at the North Playa field.
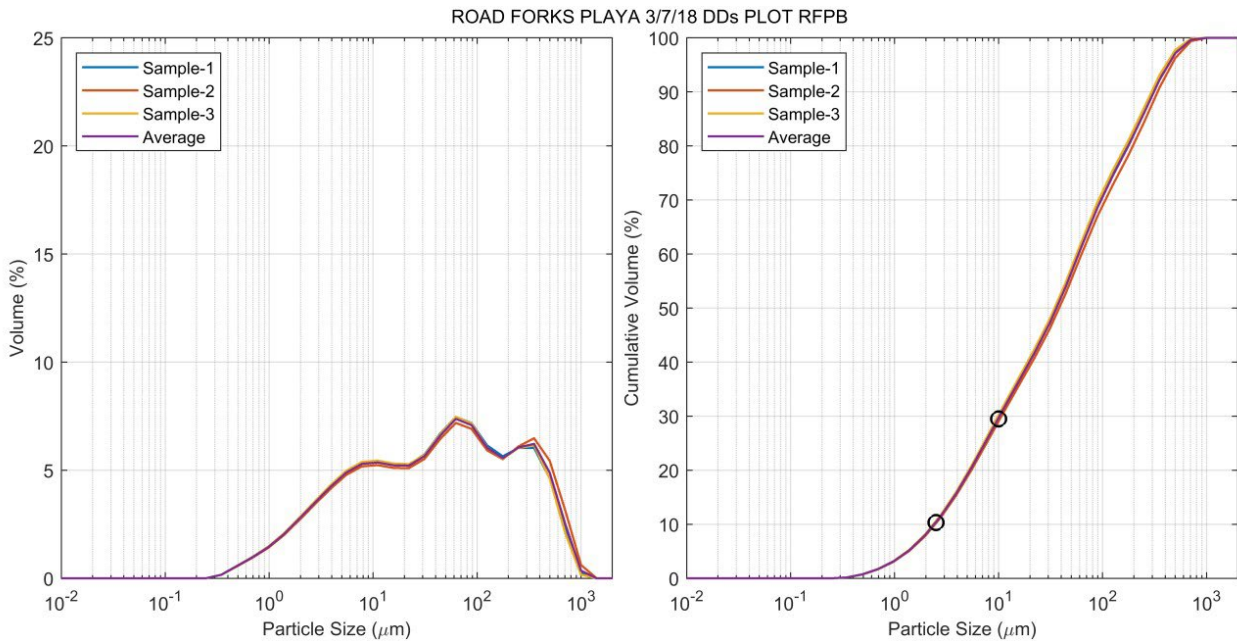
Figure 13. Grain size distribution of the soil at the Road Forks field.

AERMOD

AERMOD is a steady-state plume model with the capability to simulate dispersion from rural and urban areas, flat and complex terrain, surface and elevated releases, and multiple sources. In the stable boundary layer, the model assumes the concentration distribution to be Gaussian in both the vertical and horizonal directions (U.S. EPA, 2018a). In the convective boundary layer (CBL), the model assumes the horizontal concentration distribution as Gaussian; however, the vertical distribution is characterized with a bi-Gaussian probability density function (Willis and Deardorff, 1981). In the case of a CBL, the AERMOD model incorporates the concept of "plume lofting," whereby a portion of plume mass, released from the buoyant source, rises to and remains near the top of the boundary layer becoming mixed into the CBL (U.S. EPA, 2018a). Based on the measurements and extrapolations of those measurements, AERMOD estimates the vertical profiles of wind speed, wind direction, turbulence, temperature, and temperature gradient. In the final stage, the model uses different algorithms depending on the combinations of the input data to calculate the pollutant concentrations at the downwind receptors.

The AERMOD modeling system (Figure 14) accompanies two data preprocessors that are regulatory components, AERMET and AERMAP models. Other nonregulatory components include AERSURFACE, a surface characteristics preprocessor model; AERMINUTE, a 1-min Automated Surface Observing Stations (ASOS) wind data processor; pollutant source parameters (location and geometry) (Figure 10); and pollutant emission rate (provided by the SWEEP outputs). The AERMINUTE model processes the 1-min ASOS wind data to generate hourly average winds for input to AERMET model in stage two (U.S. EPA, 2015). The AERSURFACE model processes the land cover data from the National Land Cover Data (NLCD) to generate surface characteristics including surface aerodynamic roughness length, noontime albedo, and daytime Bowen ratio, for the use in stage three of the AERMET model (U.S. EPA, 2020). The surface aerodynamic roughness length is the height at which the mean horizontal wind speed is zero based on a logarithmic profile that is linked to the height of obstacles to the wind flow. The albedo is the percentage of total solar insolation reflected by the surface back to space. The Bowen ratio is the ratio of sensible heat flux to latent heat flux indicating the surface moisture.
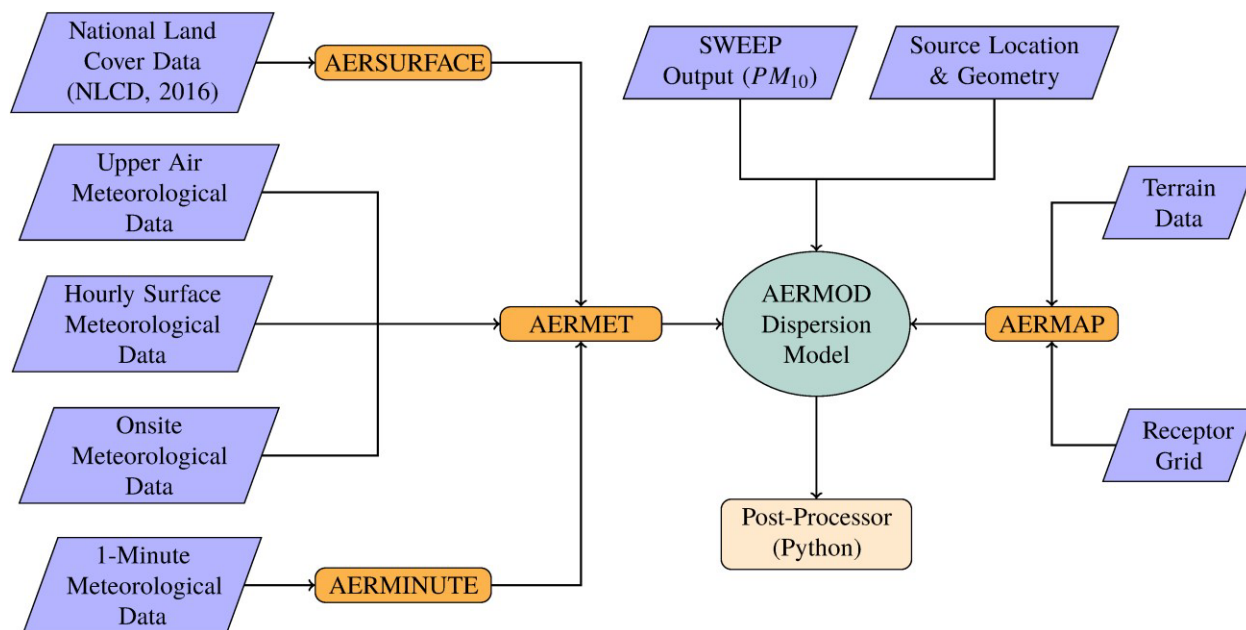
Note: AERMOD as a modeling system accompanies two data preprocessors that are regulatory components, AERMET and AERMAP models. Other nonregulatory components include AERSURFACE, a surface characteristics preprocessor model; AERMINUTE, a 1-min ASOS wind data processor; pollutant source parameters (location and geometry) (as shown in Figure 10); and pollutant emission rate (derived from the SWEEP outputs).

Figure 14. AERMOD modeling system.

The AERMET model, a meteorological data preprocessor, processes meteorological observations from hourly surface observations that are typically collected at airports by NWS and/or the Federal Aviation Administration, twice-daily upper air soundings collected by NWS, and data collected from an on-site measurement program (U.S. EPA, 2019). The AERMET model processes these three data inputs through three stages, and each stage requires a separate run. In the first stage, the surface, upper air, and on-site data are written in specific file formats, and their quality are examined. The second stage merges the data processed in stage one and the hourly average ASOS data from the AERMINUTE model into distinct 24-h periods and saves the merged data to an intermediate file. In the final stage, AERMET assimilates the merged data from stage two and surface characteristics from the AERSURFACE model to compute the boundary layer parameters (e.g., surface friction velocity, mixing height, and Monin-Obukhov length), and produces two input files required by the AERMOD model. The AERMAP model, a regulatory preprocessor for terrain data, processes terrain data (Digital Elevation Model) to generate data containing elevation and hill-height scaling factors of each receptor and source for use within the AERMOD model (U.S. EPA, 2018b).

The 1-min ASOS wind data, as an input to the AERMINUTE model for aggregation to hourly average data, were downloaded from the National Centers for Environmental Information for the Deming Municipal Airport, Deming, New Mexico, the closest ASOS site with similar environment and topographical features as Lordsburg Playa. These data are primarily used to reduce the number of calms and missing wind records in the surface data, which are the main limitations in the NWS surface meteorological data. The NLCD for 2016 including tree canopy, land cover, and impervious data at a spatial resolution of 30 m, representing the input data processed by the AERSURFACE model to create surface characteristic parameters, were acquired from the multi-resolution land characteristics (MRLCs) (Wickham et al., 2014; Yang et al., 2018). Acquiring the MRLCs was done by outlining the area corresponding to the on-site meteorological stations in Lordsburg Playa and hourly surface meteorological data source in Deming. Two types of meteorological data in addition to the hourly Deming Municipal Airport data were acquired and processed for use in AERMET. The twice-daily upper air soundings from the Tucson International Airport, which is the nearest

site and would generally be upwind of and most closely represent conditions at Lordsburg Playa, collected by NWS were used as parameters for the upper air meteorological data. The on-playa meteorological data were acquired from the NM003 and NM004 weather stations (Figure 3) provided by the New Mexico Climate Center. From the on-playa stations, wind speed, wind direction, relative humidity, air temperature, and dew point temperature data were used. In stage three, the AERMET model prioritizes the on-site data to generate an input to the AERMOD model; however, in the absence of on-site data, the model extracts the required data from NWS hourly surface observations. Since, during the dust event days of February 3, 2020, and June 5, 2020, the on-site (on-playa) NM003 and NM004 meteorological towers recorded measurements, the AERMET model used only the on-site data. For the AERMAP preprocessor model, the DEM image with the spatial resolution of 1/3 arc-second was adopted from USGS. The AERMAP model accepts a DEM if stored in GeoTIFF and uncompressed file format (U.S. EPA, 2018b). As required, the acquired compressed DEM image was converted to the GeoTIFF without compression file format. In addition, Cartesian grid networks of receptors were used at the elevation of 1.7 m above the land surface covering Lordsburg Playa and the major transportation route. The 1.7-m receptor height was determined as the average value of the current standard for eye height within the passenger car and trucks (U.S. Department of Transportation, 2006) and could also represent a reasonable standard for height for a standing human, such as a public safety officer or highway worker, inhaling ambient air. The horizontal spacing between the receptors was 150 m. The receptors were defined by the discretely placed receptor locations referenced to a Cartesian system. For the AERMOD model, this study used rotated area source, rural environment, flat terrain, ground-level release, and on-site meteorological observations. All the model runs including AERMOD, AERMET, AERMAP, AERSURFACE, and AERMINUTE models were performed using the executable files from EPA.

Results and Discussion

Field and Laboratory Data

Mean GPS locations of sites selected for PI-SWERL testing, as well as means and standard deviations of sand, silt, clay, and PM_{10} percentages of surface sediment sampled at each site, are presented in Table 5. Although some soil PSD variation is evident among the sites, the soil at the west beach site stands out as having much sandier material and much lower content of PM_{10} than any of the others. The western edge of Lordsburg Playa is close to the Peloncillo Mountains, and several small drainages empty as alluvial fans directly onto the playa surface from relatively steep terrain. In addition to the nearby steep terrain and resulting coarse sediment transport on the west side of the playa, close examination of aerial photography, satellite images, and discussions with local land managers (Trent Botkin, NMDOT, personal communication, 2020) has revealed that the dams of several small, decades-old impoundments related to mining and cattle grazing on the mountain slopes have been breached. These impoundments filled with sediment over time, and when their dams breached during seasonal rains, massive coarse sediment flows were often formed, which in this area have flowed far onto the lakebed surface (Figure 15). Prior studies systematically analyzing remote sensing imagery have suggested that these zones of contact between coarse sediments and fine playa materials play an enhanced role in initiating dust storms in the Chihuahuan Desert due to the ability of the coarse sandy materials to saltate (hop in the wind) with resultant sandblasting of the finer, wind-entrainable lacustrine sediments (Lee et al., 2009; Rivera Rivera et al., 2010).

Table 5. Mean and Standard Deviation of Longitude, Latitude, Percent Sand, Silt, Clay, and PM$_{10}$ for the Surface Sediment Samples at the PI-SWERL Test Sites

Site (Surface Class)	Mean and St. Dev.	Longitude Degrees W	Latitude Degrees N	Sand %	Silt %	Clay %	PM$_{10}$ %
AD1 (D)	Mean	108.854	32.255	17.79	69.2	12.29	41.30
	St. Dev.	1.91 E-5	8.64 E-5	1.01	1.10	0.50	1.36
AD2 (D)	Mean	108.868	32.254	28.64	57.42	13.94	42.25
	St. Dev.	3.86 E-5	3.47 E-5	4.94	4.16	3.16	7.40
AD3 (D)	Mean	108.878	32.267	18.01	70.10	11.90	45.24
	St. Dev.	8.03 E-5	5.4 E-5	1.08	1.29	1.32	3.41
AD2 (L)	Mean	108.868	32.254	30.66	57.16	12.18	37.57
	St. Dev.	1.04 E-4	3.98 E-5	5.37	7.05	1.67	2.62
RFP (L)	Mean	108.943	32.242	29.02	62.27	8.70	33.72
	St. Dev.	5.89 E-4	6.68 E-4	12.27	12.00	0.51	2.93
PC (L)	Mean	108.908	32.322	17.52	54.62	27.85	57.73
	St. Dev.	3.18 E-4	2.47 E-4	3.88	1.95	2.81	4.55
RFP (B)	Mean	108.944	32.242	56.72	36.17	7.11	25.22
	St. Dev.	—	—	—	—	—	—
EB (B)	Mean	108.832	32.333	41.33	45.35	13.32	42.55
	St. Dev.	1.65 E-4	7.11 E-5	7.13	6.13	1.70	7.06
WB (B)	Mean	108.933	32.315	84.59	12.23	3.17	10.80
	St. Dev.	1.93 E-5	4.41 E-5	13.00	10.76	2.24	8.83

Note: Surface classes are D = Delta, L = Lake, and B = Beach. — means not applicable.

Note: This figure shows erosional head cutting (left and bottom left) and flow and deposition of eroded sediments onto the playa surface (right and bottom right).

Figure 15. Aerial photograph of an area on the lower east slopes of the Peloncillo Mountains entering the west shore of Lordsburg Playa.

Mineralogy of the Lordsburg Playa surface as determined by XRD (Figure 16) showed that all samples were largely similar in composition, and principally composed of calcite, quartz, feldspars (plagioclase and potassium feldspar), analcime (a zeolite mineral), and illite/mica. Some samples also contained trace amounts of a chlorite group clay, other carbonate minerals, and other zeolites. All of these minerals are expected constituents of playa environments in the Southwest. No ore minerals (metal sulfides, oxides, or carbonates) were detectable, suggesting that primary metal compounds derived from mining activities, if present, were present only in trace amounts.
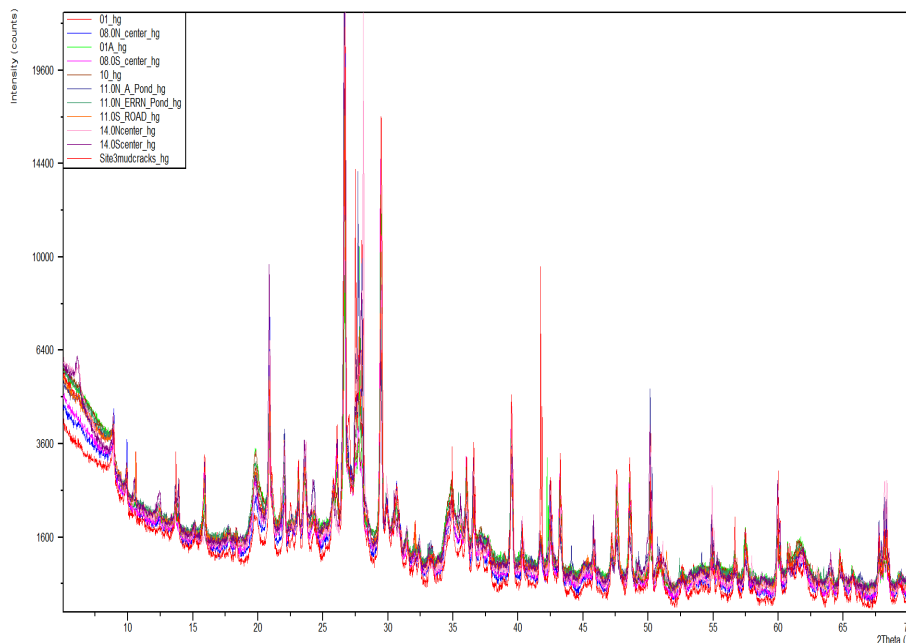
Figure 16. X-ray diffraction outputs of selected Lordsburg Playa sediments, showing similarity of composition.

The total leaching of metals in Lordsburg Playa sediments suspended in SLF, as analyzed by ICP-MS (Figure 17, Figure 18, and Figure 19), showed sample 4A, collected farthest from I-10 on the northeast shore of PC, to have the highest bioavailable Cu concentration (Figure 17[b]) of 1830 ppm. Sediment from site 3D, closest to the highway, had the highest bioavailable Pb and Zn concentrations of 20 ppm and 4690 ppm, respectively (Figure 18[b] and Figure 19[b]). Maximum likely bioavailable metal concentrations in airborne silt particles from Lordsburg Playa were therefore estimated at 4690 ppm for zinc, 1830 ppm for copper, and 20 ppm for lead. The leaching rate in the SLF varied from element to element, but for most samples, the majority of the leaching happened during the first two hours, suggesting that biological uptake of metals from Lordsburg Playa dusts through the human respiratory tract would take place promptly.

(a)   (b)
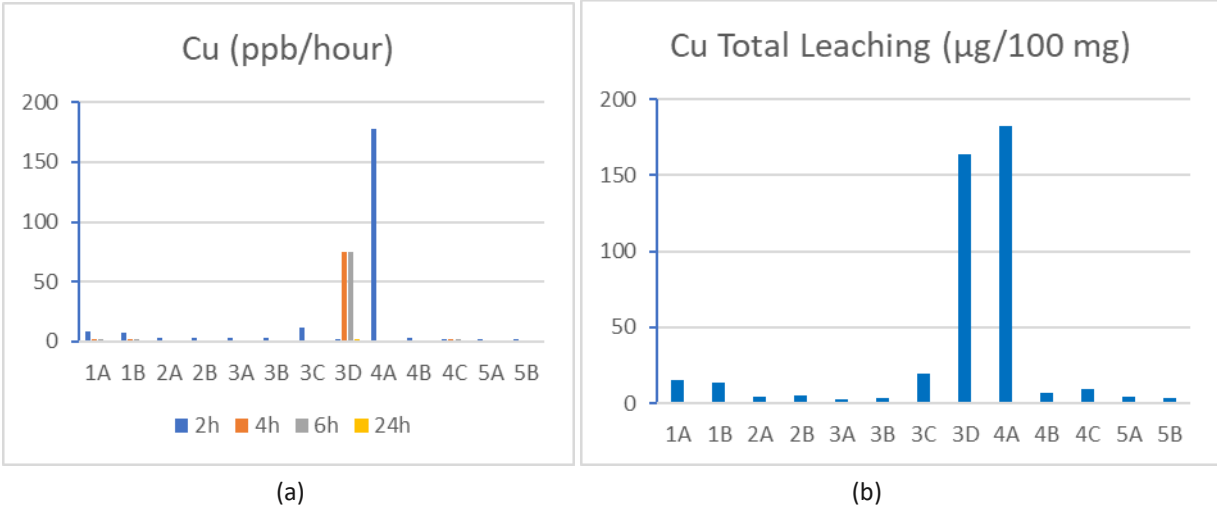
Figure 17. Comparison of (a) Cu leaching rate of Lordsburg Playa sediment samples in ppb/hour and (b) total Cu leaching for each sample.

(a)   (b)
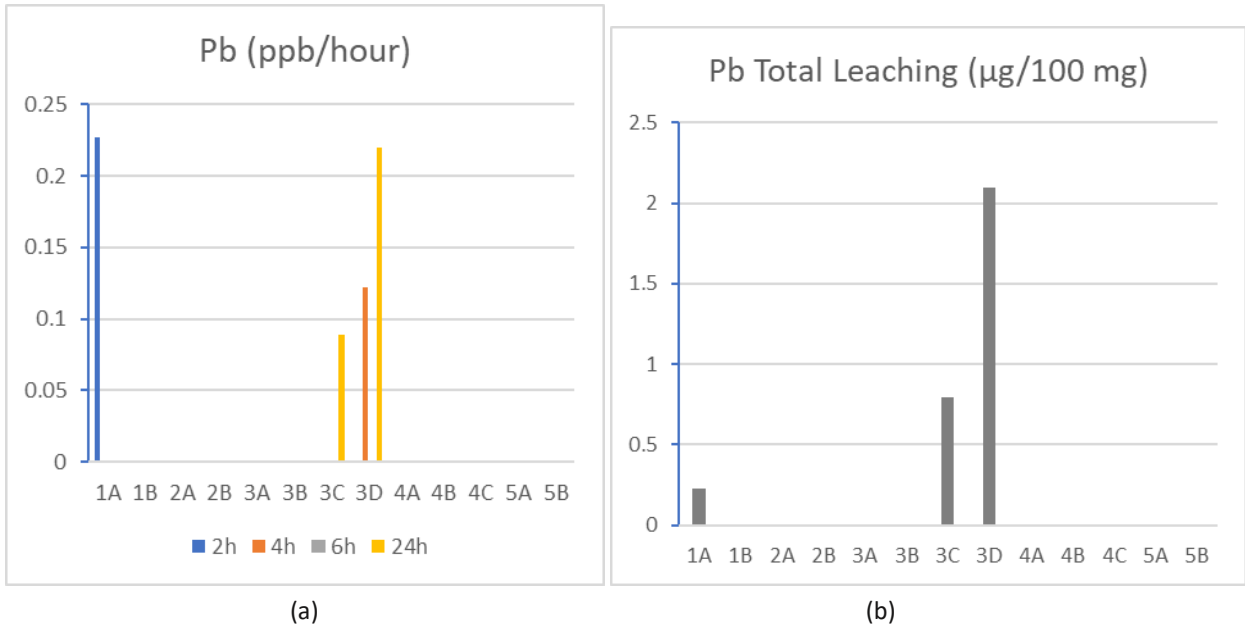
Figure 18. Comparison of (a) Pb leaching rate of Lordsburg Playa sediment samples in ppb/hour and (b) total Pb leaching for each sample.
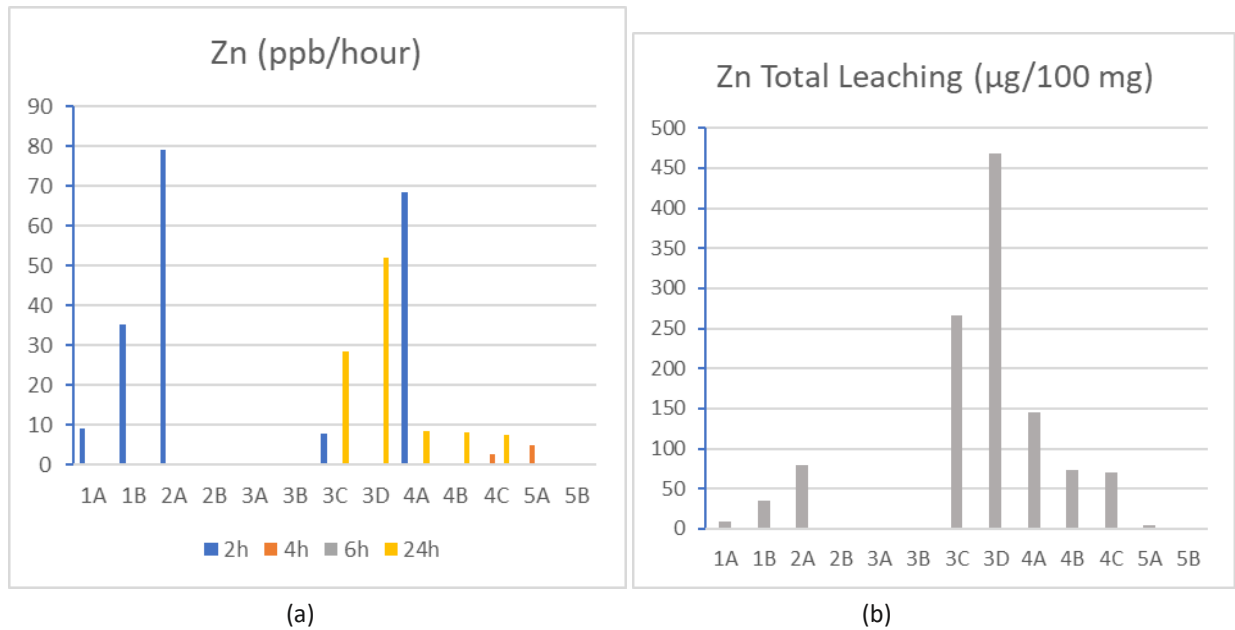
Figure 19. Comparison of (a) Zn leaching rate of Lordsburg Playa sediment samples in ppb/hour and (b) total Zn leaching for each sample.

For the PI-SWERL experiments, dust emissivity test site surface type; disturbance class; friction velocities at threshold ($u*_t$), NAAQS exceedance ($u*_{exc}$), and maximum PM_{10} flux ($u*_{max}$); and maximum vertical flux rate (MaxQ) and total PM_{10} flux (TotQ) are presented in Table 6. In general, the sites in the Animas Creek delta (D) and in the beach areas along the shorelines (B) were much more emissive of PM_{10} based on MaxQ and TotQ than lakebed sites at RFP and PC that were ephemerally flooded (L). Specifically, the undisturbed delta sites had MaxQ values between three and seven times and TotQ values between three and six times the mean value for the ephemerally flooded sites. The disturbed sites had MaxQ values between 26 and 59 times greater and TotQ values between 26 and 67 times the mean value for the ephemerally flooded sites. Sites in the delta to the south, AD1 and AD2, had apparently been cultivated at some time in the past, but all were being used for cattle grazing at the time of the field investigations. At one of the three sites, AD2, furrows had been cut between the natural soil surface to hold water and, hopefully, increase the survival of grass seedlings. The surfaces of these furrow bottoms were very similar to the hard-crust polygons found in ephemerally flooded areas, and their emission rates were also very similar. For this reason, the research team considered the furrow bottoms to be ephemerally flooded and segregated them from the other tests at this site. In a similar manner, one of the tests at RFP was performed on a mantle of aeolian sand that resembled a beach deposit, which was classified as a beach class surface. With these exceptions, the replicate spots in each site were very uniform in surface characteristics, and all PI-SWERL test derived data were used to calculate the means presented in Table 6.

Table 6. Surface Class (Delta, Lake, or Beach), Disturbance Class (Undisturbed or Disturbed), and Mean and Standard Deviation of Threshold Friction Velocity ($u*_t$), Friction Velocity at Which the NAAQS Standard for PM_{10} Would Be Exceeded in a 30 m Tall Column of Air ($u*_{exc}$), Friction Velocity at Which the Maximum Rate of PM_{10} Vertical Flux Is Observed ($u*_{maxQ}$), the Maximum Rate of PM_{10} Vertical Flux Observed (Max Q), and the Total PM_{10} Vertical Flux for the Nine-Minute PI-SWERL Test (Tot Q) of Each Sample Site

Site	Surface Class	Disturbance Class	Mean and St. Dev.	$u*_t$ (m s^{-1})	$u*_{exc}$ (m s^{-1})	$u*_{maxQ}$ (m s^{-1})	Max Q (ug m^{-2} s^{-1})	Tot Q (ug m^{-2})
AD1	D	U	Mean	0.31	0.80	0.81	1325.48	84217
			St. Dev.	0.02	0.02	0.00	919.87	69106
AD1	D	D	Mean	0.31	0.62	0.81	11030.94	845554
			St. Dev.	0.02	0.07	0.01	5498.17	5168485
AD2	D	U	Mean	0.26	0.74	0.80	3098.75	193221
			St. Dev.	0.05	0.12	0.02	2021.42	131854
AD3	D	U	Mean	0.24	0.60	0.80	1248.26	999201
			St. Dev.	0.05	0.15	0.02	8697.52	832504
AD3	D	D	Mean	0.31	0.50	0.68	24977.63	2226249
			St. Dev.	0.02	0.03	0.05	1778.07	682823
AD2	L	U	Mean	0.31	—	0.80	223.60	16733
			St. Dev.	0.01	—	0.00	36.49	2287
RFP	L	U	Mean	0.36	—	0.81	476.06	45648
			St. Dev.	0.06	—	0.00	406.79	77958
PC	L	U	Mean	0.56	0.81	0.80	561.84	36857
			St. Dev.	0.10	—	0.02	717.75	49034
RFP	B	U	Mean	0.39	0.77	0.81	2450.36	288993
			St. Dev.	—	—	—	—	—
EB	B	U	Mean	0.30	0.72	0.81	7561.78	788012
			St. Dev.	0.10	0.08	0.00	12282.01	1266773
WB	B	U	Mean	0.28	0.50	0.80	17182.49	2727300
			St. Dev.	0.04	0.05	0.02	6844.97	1084141

Note: — means not applicable.

Analysis of the NM003 and NM004 weather data obtained from the New Mexico Climate Center indicated that March, April, and May have greater 15-min mean wind speeds than the other months. This finding is consistent with the large-scale spring weather patterns in the Chihuahuan Desert and southern New Mexico, and represents the season with the greatest number of synoptic-scale dust storms covering large areas (Novlan et al., 2007; Rivera Rivera et al., 2010). When gusts are considered, however, frequencies of exceedance for the threshold wind speeds increase for all months, especially during the monsoon months of June, July, and August, in which afternoon convective storms may form and produce strong downdrafts and outflow winds. In general, December, January, February, and September are the months with the calmest winds at Lordsburg Playa.

Surface physical characteristics at the PI-SWERL test sites, such as texture, structure, and the presence or absence of an undisturbed crust, had a significant impact on $u*_t$ ($p < 0.0001$) but not $u*_{exc}$ ($p = 0.1658$) or $u*_{max}$ ($p = 0.7975$). PM_{10} emissions, on the other hand, were greatly affected by surface physical characteristics, with the mean MaxQ of the beach deposits being more than two times that of undisturbed delta soil surfaces, whose mean MaxQ was in turn over an order of magnitude greater than the ephemerally flooded lacustrine deposits ($p = 0.0018$). Similarly, the TotQ during the test was highly influenced by surface physical characteristics, with the mean TotQ of beach deposits being over three times greater than the mean for undisturbed delta soil surfaces, which had mean TotQ of more than an order of magnitude greater than the mean for ephemerally flooded lacustrine deposits ($p = 0.0003$).

Although disturbance only influenced one of the u*, specifically $u*_{exc}$, values significantly, it had a very significant effect on the maximum vertical flux of PM_{10} (MaxQ) during the testing, with disturbed sites having mean emission rates of nearly an order of magnitude greater than the undisturbed sites (p = 0.0131). Similarly, the total PM_{10} emitted by the disturbed sites was more than an order of magnitude greater for the disturbed sites than the undisturbed (p = 0.0266). These trends of increased PM_{10} emissions with surface crust disturbance are consistent with experimental findings at other wind-erodible playas (Cahill et al., 1996; Baddock et al., 2011b; Klose et al., 2019) and desert surfaces (Van Pelt et al., 2017; Klose et al., 2019) in the North American drylands, specifically including the effects of livestock activity (Baddock et al., 2011b) and off-highway vehicles (Goossens and Buck, 2009) in increasing dust emission through breakage of surface crusts (Figure 20). The variance among disturbed sites for both these measures was much greater than for undisturbed sites. Undisturbed sites were more predictable in their emission rates and total emissions than disturbed sites, which indicates the necessity of limiting disturbance and breakage of natural dryland soil crusts in land management plans for mitigating the dust hazard, especially in areas devoid of vegetation where aerodynamic roughness lengths are very small.

Note: Photo by Marcos Mendez.

Figure 20. Polygonal surface crusts on playa showing highly erodible, wind-entrainable material exposure beneath the crusts where they are broken, removed, or disturbed.

In general, the three sites on the Animas Creek delta, AD1, AD2, and AD3, had soils that were fine textured with shallow surface crusting. At site AD1, the movement of cattle along a fence line had disturbed the surface very close to undisturbed PI-SWERL replicate test spots, and the researchers tested them as a subset of the site tests. Similarly, at site AD3, side-by-side undisturbed and tire-track-disturbed surfaces allowed the research team to assess the effects of crustal disturbance on PM_{10} emissions and related critical friction velocity parameters. The team found no differences in $u*_t$ related to disturbance of the soil crust at either AD1 or AD3 (p = 0.9797), but the friction velocities at which the NAAQS PM_{10} standard of 150 µg m^{-3} would be exceeded in a 30-m atmospheric column, $u*_{exc}$, were significantly greater for undisturbed soil crusts than for disturbed (p = 0.0305). The mean values of $u*_{exc}$ for the disturbed spots tested at AD1 and both undisturbed and disturbed spots at AD3, when adjusted to wind speed equivalents, were among very few with less than gale force (< 17.5 m s^{-1}) velocities, although frequencies of exceedance during the five years of wind speed data collection were only about 0.2 percent and 1.4 percent, respectively, for maximum wind gusts and much less than that for 15-min means. The undisturbed surface crust at AD3 was very fragile, and during a PI-SWERL test of these spots, it was not uncommon to see a very rapid rise in PM_{10} vertical flux rates. Such rapid increases would be consistent with the visual observation at the end of a test where the shear force had displaced a polygon of crust and revealed easily entrainable sediments below the surface (as also shown in Figure 20), which has been noted as a key process threshold for increasing dust emission at other playas (Cahill et al., 1996). Disturbance also did not significantly influence the friction velocities at which the maximum vertical flux was observed, $u*_{max}$ (p = 0.6491), although the variances of all friction velocity values were much smaller for the undisturbed sites, demonstrating the stabilizing

influence of soil crusting. The researchers estimate from 15-min mean wind speeds that the threshold wind speed at which PM_{10} entrainment would be initiated would be exceeded approximately 5 percent of the time for sites at AD1, the lakebed surface at AD2, and the disturbed surface at AD3. Other delta surface sites had higher frequencies of exceedance including approximately 10 percent of the time for the undisturbed delta surface at AD2 and 13 percent of the time for the undisturbed surface at AD3. When maximum gusts are considered, the frequencies of exceedance for threshold wind speed for PM_{10} entrainment approximately double. Only the AD3 disturbed site had 2-m U_{maxQ} values low enough that gusts have exceeded this wind speed more than once or twice in the last five years, but this is a notable artifact of early test terminations to protect the optical bench of the nephelometer.

Naturally crusted (undisturbed) spots at site AD2 had lower emission rates and total dust emissions than the undisturbed spots at AD1 and AD3. However, the ephemerally flooded furrows had emission rates and totals an order of magnitude smaller than the naturally crusted surfaces. These furrows had highly indurated polygonal crusts very similar to the ephemeral lakebeds. Although it was less evident with the disturbed site tests, there is a limitation of PM_{10} supply in the soils of the Animas Creek delta. Figure 21 shows a drop of emission rate following each local maximum as the RPM, and resulting shear force on the surface caused by the PI-SWERL rotating ring was increased and then held steady.
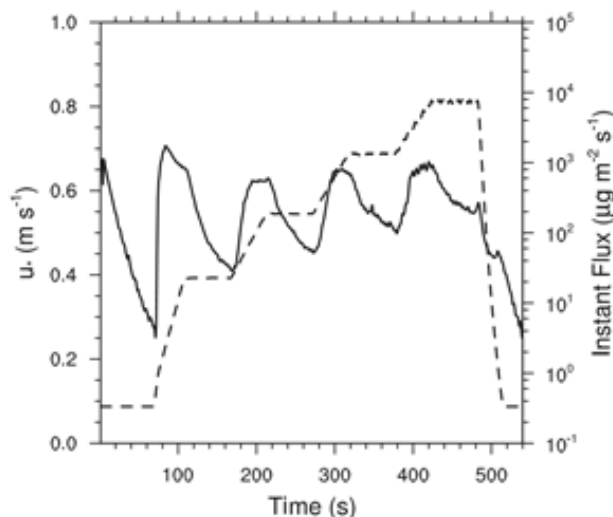
Note: The dashed line represents the friction velocity (u*), and
the solid line is instantaneous vertical flux of PM_{10}. This test
was from an area that is ephemerally flooded (L).

Figure 21. PI-SWERL test response curve showing a PM_{10} supply limitation.

Playa beach deposits at the eastern (EB) and western (WB) ends of the pipeline service road that bisects the large playa surface just north of I-10 were tested and found to be highly dust emissive, especially the WB end. The $u*_t$ means of these sites were not significantly different (p = 0.6630) and were about the same as those found for undisturbed surfaces in the Animas Creek delta but exhibited greater variance. The 2-m, 15-min mean wind speeds exceeded the estimated threshold for PM_{10} entrainment at EB and WB approximately 6 percent and 8 percent of the time periods, respectively, and when gusts were considered, the threshold was exceeded approximately 15 percent and 18 percent of the time, respectively. The mean $u*_{exc}$ for WB was significantly lower than that for EB (p = 0.0112). The 2-m, 15-min mean wind speed that would exceed the threshold for NAAQS levels would occur less than 0.01 percent of the time for EB and approximately 0.16 percent of the time for WB, and for gusts, the threshold would be exceeded 0.03 percent and 1.37 percent of the time, respectively. Despite the significantly lower $u*_{exc}$ for WB, the mean $u*_{max}$ for WB, although much more variable, was not significantly lower than the

mean for EB (p = 0.3847). Although the mean maximum PM_{10} flux rate for WB was more than twice that for EB, high variance at both sites precluded any significance in the difference (p = 0.2202). More side-of-playa effect was found for the mean total flux of PM_{10} (TotQ) in which the mean total for WB was nearly four times that for EB (p = 0.0589). The primary test response difference between EB and WB was that the tests conducted at WB did not exhibit any apparent supply limitation (Figure 22) and maintained their emission rates until the RPM and resultant shear stress of the PI-SWERL rotating ring increased to the next level and was held. At EB, supply limitation was apparent at lower values of friction velocity at the early time steps of the test and only overcame supply limitation at higher values of friction velocity. Like many of the test surfaces on the Animas Creek delta, the spots tested at WB also had a mean value of $u*_{exc}$ that, when converted to wind speed equivalents, was also less than gale force. Events with wind speeds in excess of gale force for extended periods of time are rare at inland mountainous locations. Thus, most of the dust entrained will, with the exception of gusts or short periods in which strong pressure gradients are being equilibrated, be entrained with less than gale force velocities.
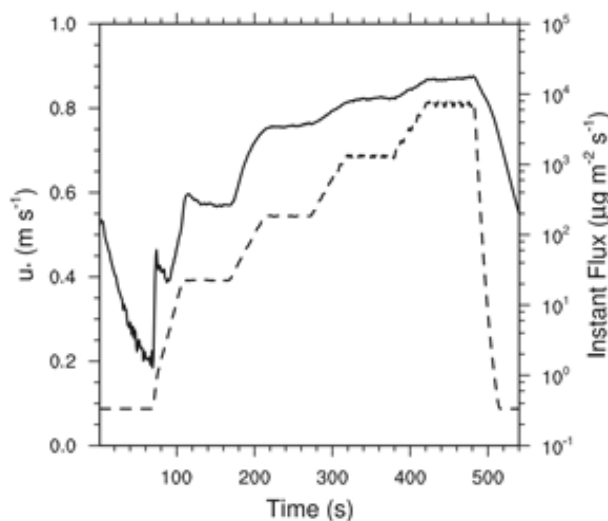
Note: The dashed line represents friction velocity (u*), and the solid line is instantaneous vertical flux of PM_{10}. This test was from the western beach area.

Figure 22. PI-SWERL test response curve showing no PM_{10} supply limitations once threshold friction velocity has been exceeded.

The two sites tested that represent the parts of the lakebed that may become ephemerally flooded during and after the rainy season (Eibedingil et al., 2021) included the small but problematic RFP just south of I-10 near the western edge of the main Lordsburg Playa and a site north of the pipeline access road very near the center of the northern half of the large PC. At the RFP test site, four ephemerally flooded surfaces were tested, as well as one that had a mantle of aeolian sand that the researchers classed as a beach type surface. At the PC test site, nine tests were conducted. Values of mean observed $u*_t$ were more than 50 percent greater than for the beach and delta deposits. The tests conducted on the ephemerally flooded surface at RFP did not result in a value of $u*_{exc}$ that would have exceeded the NAAQS standard for PM_{10}. From the NM003 and NM004 weather station data, the 2-m, 15-min mean wind speed would have exceeded the threshold for PM_{10} entrainment at the RFP and PC test sites 2.3 percent and 0.02 percent of the time, respectively; considering gusts, the frequencies would increase to 8.3 percent and 0.6 percent of the time, respectively.

At the PC site near the center of the playa, only one of the nine replicate test spots resulted in an NAAQS standard exceedance for PM_{10} in a 30-m column of atmosphere, and that value was near the maximum of friction velocities recorded during all phases of testing at all sites. The equivalent wind speed would have exceeded 23 m s^{-1}, and this

wind speed was only exceeded by maximum gusts twice in the five years of record. The mean value of $u*_{max}$ for these surfaces was slightly lower than that noted for the other two surface types and had greater variance. The mean maximum vertical flux of PM_{10} from ephemerally flooded surfaces was less than 500 µg m^{-2} s^{-1}, and the mean total PM_{10} flux during the 9-min test was less than 37 mg m^{-2}.

Although the ephemerally flooded lacustrine deposits occupy the predominant surface area on the geomorphically complex Lordsburg Playa, at least during the field testing, they exhibited lower PM_{10} emissivities than would be necessary to obscure visibility along I-10, which is due to the limited abrader material on the solid playa surfaces at that time. Sand from beach areas or coarse sediment flows saltating downslope (such as those flowing into the playa from the surrounding uplands) and/or downwind across large areas of the indurated clay-rich crust, or disturbance by crust crushing activities such as off-road vehicle traffic or livestock grazing, could potentially change this situation and increase dust emissivity beyond those measured in this project. One of the limitations of the PI-SWERL is the inability to introduce abrading (saltating) sand, and this limitation may have limited PM_{10} emission observations.

Numerical Modeling

SWEEP

The SWEEP model simulated likely maximum soil loss from wind erosion in terms of total, saltation/creep, suspension, and PM_{10} from the North Playa and RFP fields for the dusty days of February 3 and June 5, 2020, and results are presented in Figure 23 through Figure 26. The North Playa fields emitted 1245.92 and 1664.73 metric tons of PM_{10} during the February 3 and June 5 dust event days, respectively. The Road Forks fields discharged 30.16 kg and 50.75 kg of PM_{10} on the February 3 and June 5 dust event days, respectively. The hourly PM_{10} emission rate for use in the AERMOD model was also generated by SWEEP. In all four scenarios, the soil loss started at 11:00 local time, primarily influenced by the magnitude of the wind speed indicating that during this time the friction velocity started to exceed the static friction velocity threshold. Prior to this time, simulated soil loss was zero in all soil loss modes.

During the dust event day of February 3, 2020, the simulated soil loss from North Playa showed a reasonably normal distribution, peaking at around 17:00 with around 0.41 g m^{-2} sec^{-1} soil loss (Figure 23). During this time, in the largest fields, the saltation/creep, suspension, and PM_{10} soil loss was around 0.05, 0.35, and 0.015 g m^{-2} sec^{-1}, respectively; in the smallest field (Field 1), the loss was 0.19, 0.20, and 0.08 g m^{-2} sec^{-1}, respectively. The total loss (per area unit time) was the same across all subfields irrespective of geometry because the biomass, soil properties, and meteorology inputs to the SWEEP model were the same. However, the other three soil loss modes (saltation/creep, suspension, and PM_{10}) showed variability with the length of the fields. The suspension and PM_{10} soil losses increased with the increase in field lengths because the suspension component continues to increase with downwind distance and the sources for suspension-size are usually active over the entire field (USDA-ARS, 2007). In addition, this component has greater transport capacity than that of the saltation/creep components. On the other hand, the saltation/creep modes showed greater soil loss in the shorter fields due to the property of the saltation/creep components to reach transport capacity at a shorter distance by using all the available wind disturbance from the wind speed. Thus, in the shorter fields, the saltation/creep components may reach capacity within that allowable short distance and discharge more soil than the suspension mode. For example, for Field 1 the saltation/creep loss reached the maximum soil emission at around 200 m downwind from the southwest edge of the field. However, the suspension and PM_{10} soil discharge reached its maximum value at the other end of the field (at 401 m).
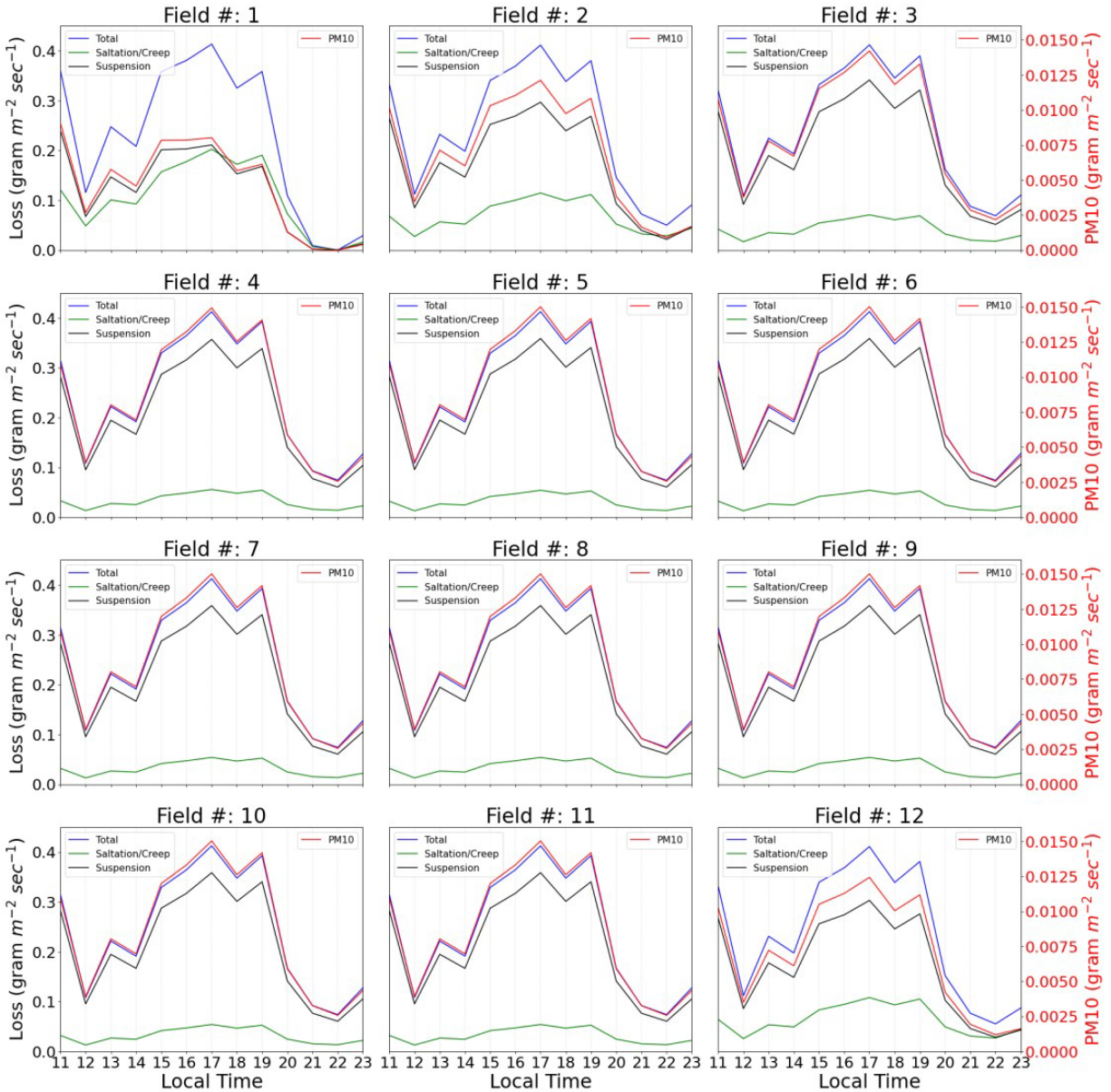
Note: The left y-axis represents the total, saltation/creep, and suspension loss; the right y-axis (twin axis) represents PM_{10}.

Figure 23. SWEEP simulated soil loss in terms of total, saltation/creep, suspension, and PM_{10} from the North Playa field during the dust event of February 3, 2020.

On June 5, 2020 (Figure 24), the North Playa field emitted much greater amounts of soil dust than on February 3, 2020, due to a greater wind speed. The loss was greatest at 15:00 in all soil loss modes. During that time, in the longer fields (Field 2 to 9), the saltation/creep, suspension, and PM_{10} losses were 0.22, 1.5, and 0.063 g m^{-2} sec^{-1}, respectively; in the shortest field (Field 1), the loss was 0.58, 1.13, and 0.04 g m^{-2} sec^{-1}, respectively. For Field 1, the saltation/creep soil discharge reached a maximum at around 400 m from the southeast edge of the field. However, the suspension and PM_{10} losses reached a maximum at the other end of the field (at 619 m). Similar to the dust event of February 3, 2020, the dusty day of June 5, 2020, also showed greater soil loss through saltation/creep modes in the shortest fields. The RFP field is much smaller in size than the North Playa field, and thus during the two dusty days, it generated less simulated soil loss. However, due to the combination of its position along the dominant southwesterly wind direction during the windy spring season and its location immediately adjacent to

31

I-10, this field poses a serious threat to public health and safety at Lordsburg Playa. During the dust event on February 3, 2020, the Road Forks subfields showed a multimodal distribution of soil loss across all subfields, peaking at 16:00 (Figure 25). Saltation/creep components dominated the soil loss across five subfields (Fields 1, 2, 3, 8, and 9) due to their shorter area length. In the longest field, saltation/creep, suspension, and PM_{10} components of soil emission were 0.13, 0.22, and 0.09 g m^{-2} sec^{-1}, respectively; in the shortest field, the amounts were 0.23, 0.009, and 0.003 g m^{-2} sec^{-1}, respectively. During the convective dust event on June 5, 2020 (Figure 26), similar to February 3, 2020, soil loss experienced a multimodal distribution, with the creep/saltation component dominating in the shorter fields. However, the rates of soil loss were greater during the June 5 event. In the longest field, the discharged soil through saltation/creep, suspension, and PM_{10} reached 0.25, 0.41, and 0.18 g m^{-2} sec^{-1}, respectively.
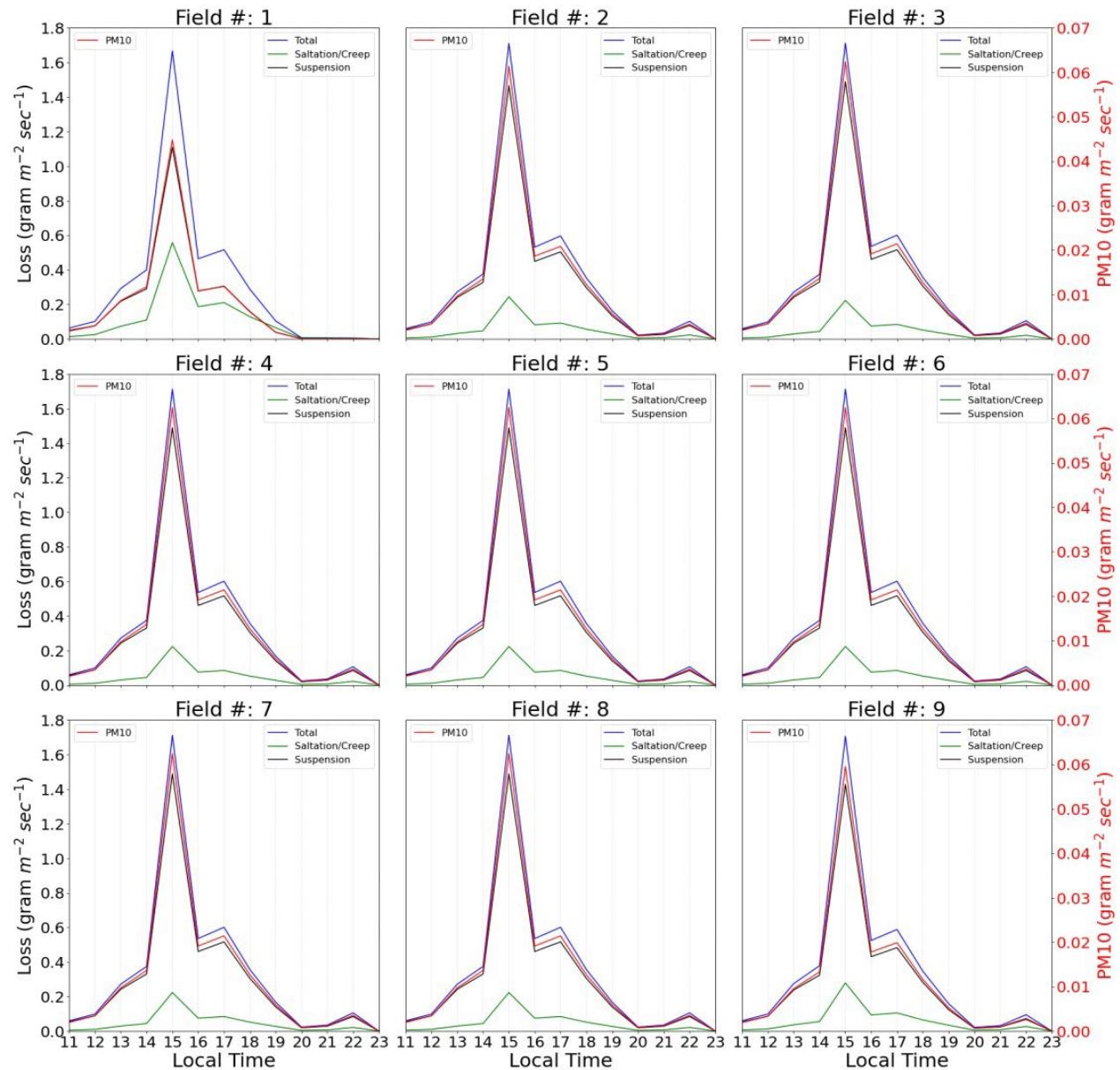
Note: The left y-axis represents the total, saltation/creep, and suspension loss; the right y-axis (twin y-axis) represents PM_{10}.

Figure 24. SWEEP simulated soil loss in terms of total, saltation/creep, suspension, and PM_{10} from the North Playa field during the dust event of June 5, 2020.
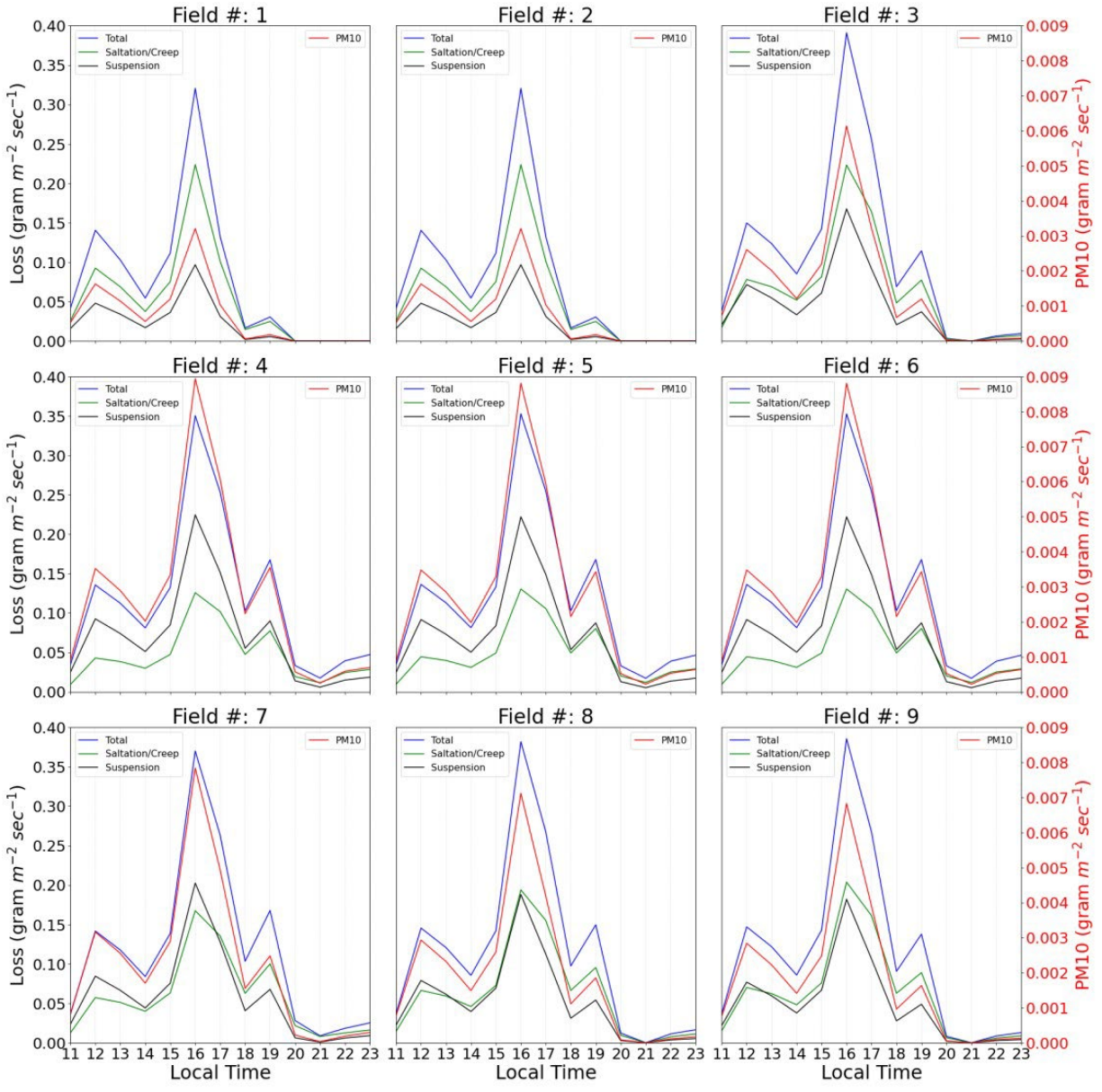
Note: The left y-axis represents the total, saltation/creep, and suspension loss; the right y-axis (twin y-axis) represents PM$_{10}$.

Figure 25. SWEEP simulated soil loss in terms of total, saltation/creep, suspension, and PM$_{10}$ from the Road Forks field during the dust event of February 3, 2020.
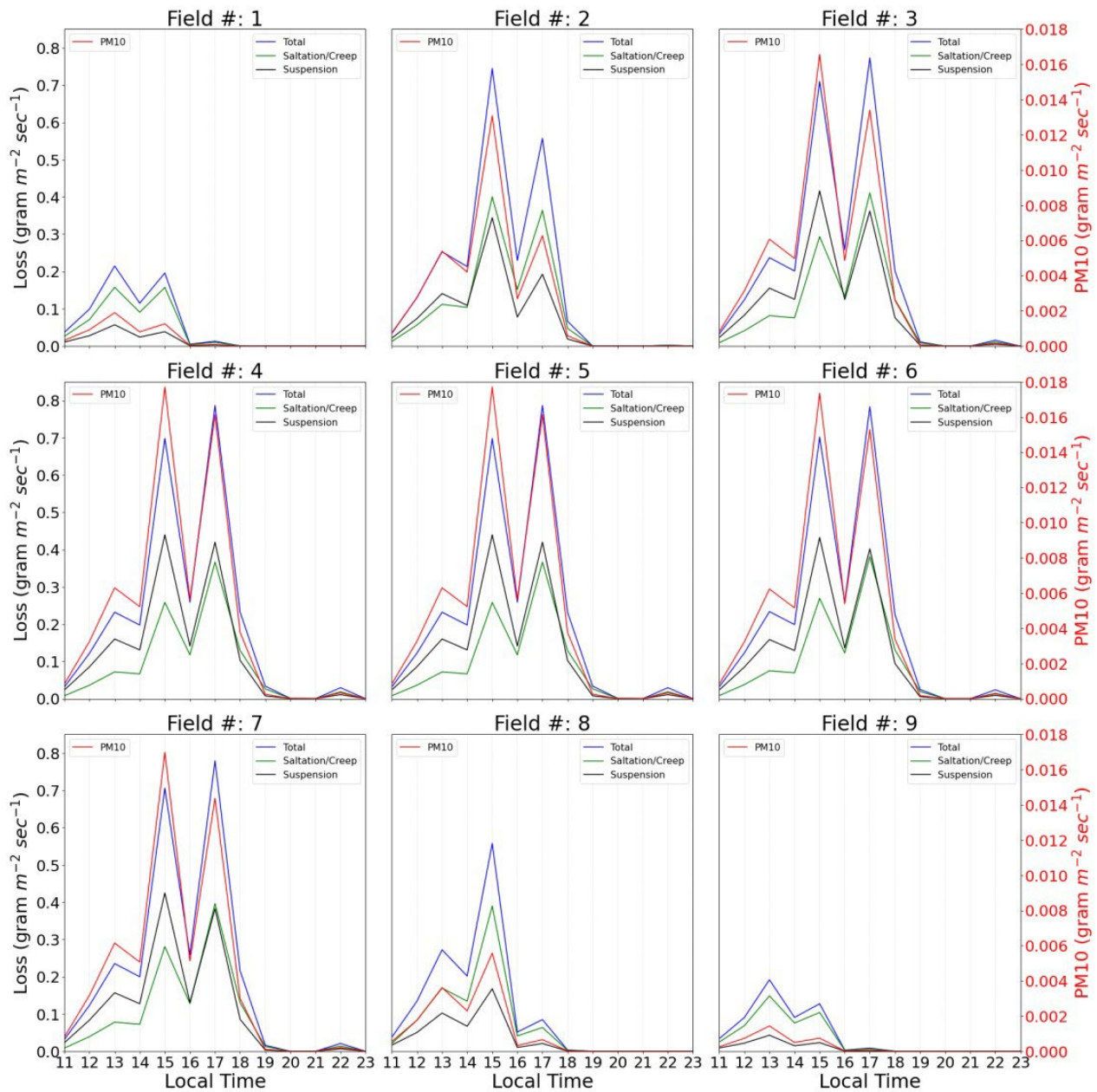
Note: Left y-axis represents the total, saltation/creep, and suspension loss; right y-axis (twin y-axis) represents PM₁₀.

Figure 26. SWEEP simulated soil loss in terms of total, saltation/creep, suspension, and PM₁₀ from the Road Forks field during the dust event of June 5, 2020.

AERMOD

The hourly dispersion of PM$_{10}$ over Lordsburg Playa, simulated by the AERMOD modeling system driven by the SWEEP model outputs for the dust event days of February 3, 2020, and June 5, 2020, are presented in Figure 27 and Figure 28, respectively. These dispersions represent PM$_{10}$ concentration at the receptor with a height of 1.7 m above the playa surface. The hourly concentrations of PM$_{10}$ that reached the interstate highway during these dust events were determined in terms of time and space. The exposure of I-10 motorists, highway workers, and public safety personnel—including those stopped on the right of way during or after a dust storm or traffic halt—to this particulate pollution will affect public safety and health by reducing visibility and air quality. As expected, the concentrations of dust and PM$_{10}$ were higher at and near the source areas, and gradually decreased with

increasing distances downwind. This finding also demonstrated that when the playa is exposed to high winds, I-10 and its right of way can be impacted by particulate matter pollution from all wind directions. The size of the respective fields (area affected by wind erosion) is also an important factor that determines the amount of particulate matter channeled to the highway.
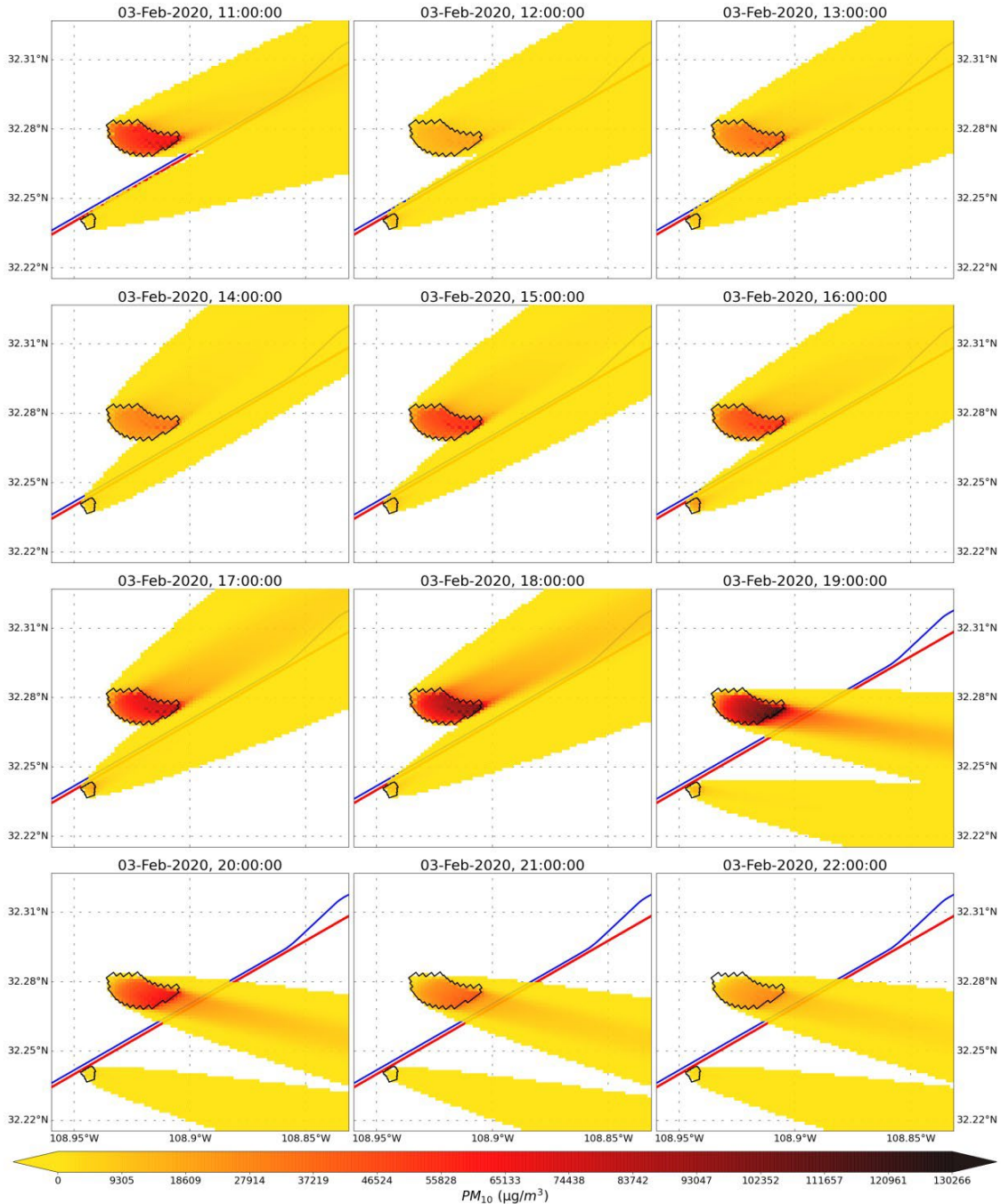
Notes: The two closed polygons represent the PM_{10} sources. The red and blue lines represent I-10 and Union Pacific Railroad, respectively.

Figure 27. Hourly dispersion of PM_{10} over Lordsburg Playa simulated by AERMOD for the dust event day of February 3, 2020.
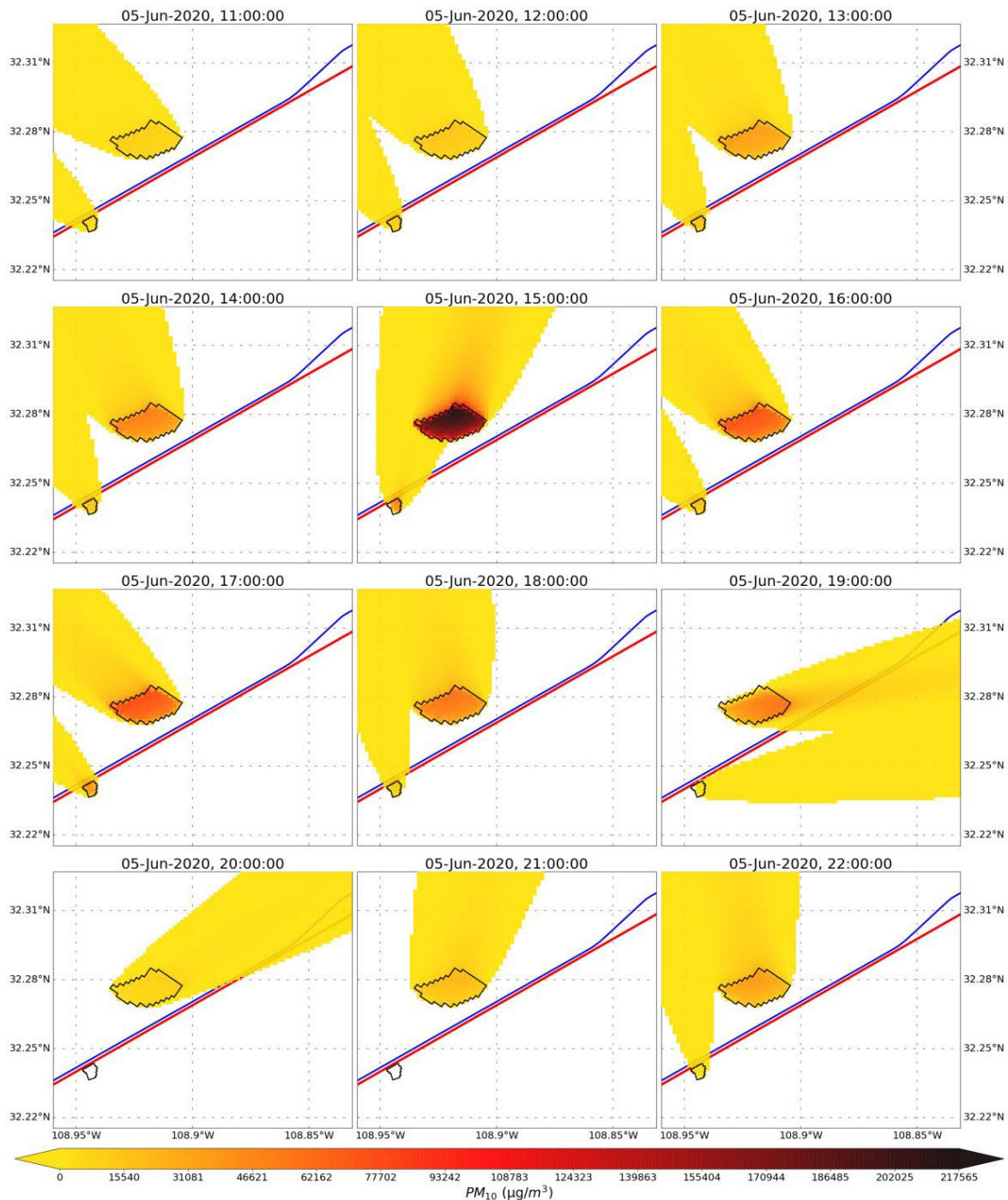
Notes: The two closed polygons represent the PM$_{10}$ sources. The red and blue lines represent I-10 and Union Pacific Railroad, respectively.

Figure 28. Hourly dispersion of PM$_{10}$ over Lordsburg Playa simulated by AERMOD for the dust event day of June 5, 2020.

The highest hourly concentration of PM$_{10}$ estimated during the dust event day of February 3, 2020, was around 130,266 μg/m^3 (Figure 27), and that was 866-fold the U.S. EPA daily NAAQS concentration limit for PM$_{10}$ of 150 μg/m^3. This magnitude of PM$_{10}$ concentration was observed at and near the North Playa field. Although this may initially appear to be an astonishingly high concentration of particulate matter, other AERMOD studies

predicted and confirmed extreme concentrations of PM_{10} at a downwind distance from playa dust sources. For example, Ono et al. (2011) simulated 60,000 μg/m³ of hourly PM_{10} concentration at the Mono Lake Playa in California using the AERMOD modeling system during the dust storm of November 20, 2009, which was validated by a ground-based instrument reaching 65,112 μg/m³ of maximum hourly PM_{10} concentration during that day. Although during the February 3, 2020, event at Lordsburg Playa the prevailing wind direction was from the southwest, the greatest concentrations of PM_{10} on the highway were directed from the northwest during the evening hours. This observation was supported by the visibility data from the NM003 meteorological site and webcam photos from the NMDOT traffic cameras at Mile Post 11 in Lordsburg Playa (Figure 29 and Figure 30). Due to blowing dust, the minimum hourly visibility measured at the NM003 meteorological site on February 3, 2020, dropped abruptly from 12.43 mi to 1.03, 2.35, and 5.57 mi at 15:00, 16:00, and 17:00, respectively. The webcam photos (Figure 30) also display blowing dust that moves from the North Playa field toward the camera between 15:31:23 and 15:39:23, confirming the AERMOD properly simulated PM_{10} emission around 15:00 and 16:00. The greatest hourly concentration blowing toward the highway was recorded at 19:00 and originated from the North Playa field.
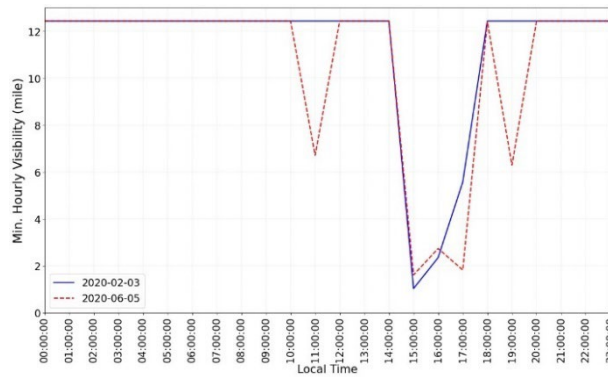
Figure 29. Minimum hourly visibility for the dust event days of February 3, 2020, and June 5, 2020, from the NM003 meteorological station.
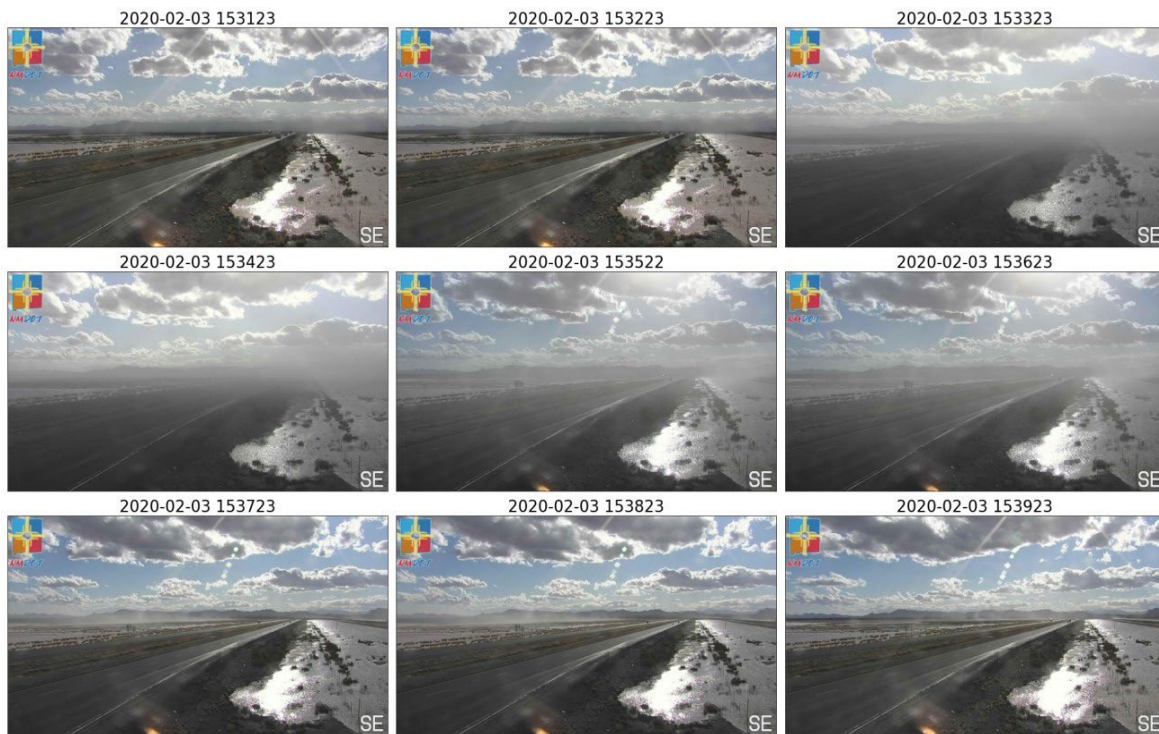
Figure 30. Blowing dust recorded by webcam photos at Lordsburg Playa from NMDOT traffic cameras at Mile Post 11 on February 3, 2020.

On June 5, 2020, the maximum hourly PM_{10} concentration was around 217,565 $\mu g/m^3$, and the dominant wind direction was southwesterly. This maximum concentration was recorded at 15:00. At this hour, the simulated emission originated from the North Playa field and advected to the north (Figure 28). Thus, during this hour, the impact of PM_{10} pollution from the North Playa field on the transportation route was minimal. However, the PM_{10} emission from the Road Forks field channeled directly toward the transportation route and may have impaired visibility. Reinforcing this observation, the NM003 meteorological site (Figure 3) also exhibited a visibility of 1.61 mi (Figure 29), a sudden drop from 12.43 mi at 14:00. Although the North Playa field discharged greater PM_{10} emission, due to the prevailing wind direction, the emission's impact on transportation infrastructure from this field was lesser. Overall, the particulate pollution to I-10 was mainly advected from the Road Forks field. The webcam photos from the NMDOT traffic camera confirmed these findings (Figure 31). At 17:00, the AERMOD simulated PM_{10} emitted from both fields blowing toward the northeast, although the emission from the North Playa field was greater. The webcam photos captured between 17:22:23 and 17:29:23 also showed dust blowing from both fields, with the blowing dust thicker on the north side of I-10.
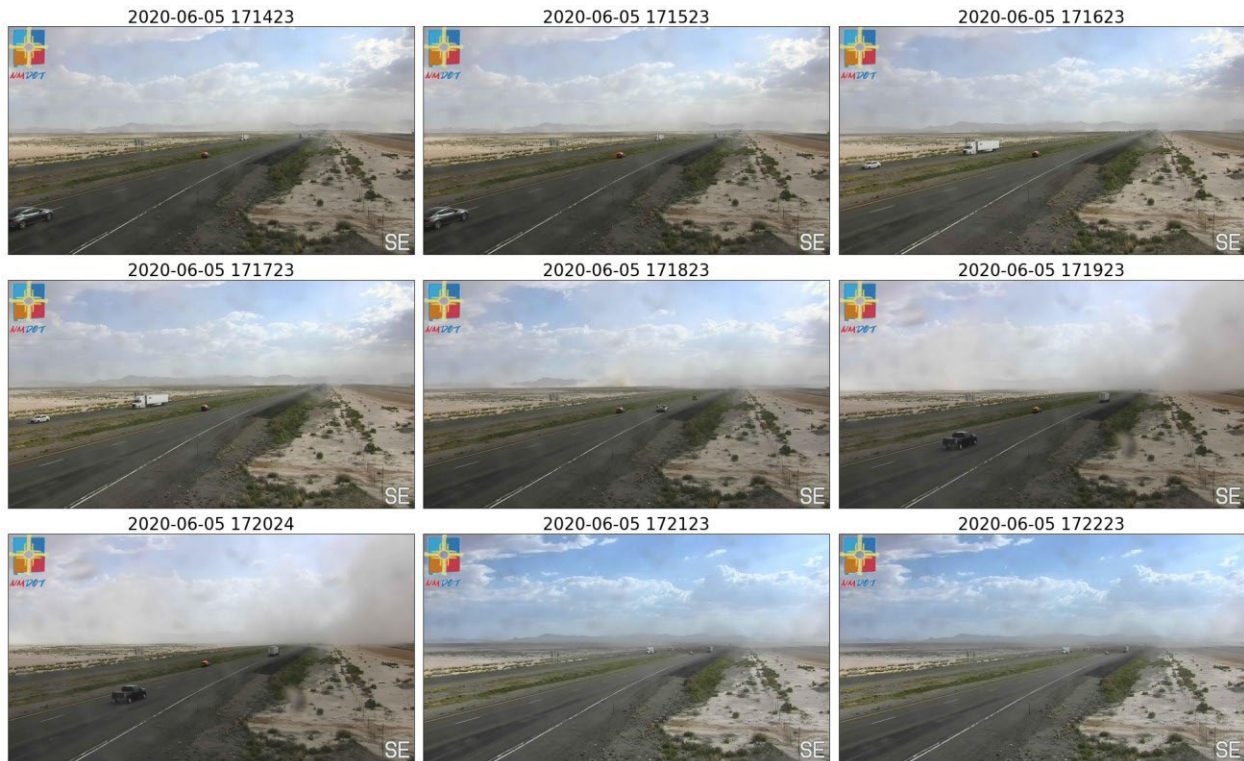
Figure 31. Blowing dust recorded by webcam photos at Lordsburg Playa from NMDOT traffic cameras at Mile Post 11 on June 5, 2020.

In summary, the soil losses from wind erosion (dust and sand emission) in terms of total, saltation/creep, suspension, and PM_{10} components were simulated using the SWEEP model for the dust event days of February 3 and June 5, 2020. The North Playa fields emitted 1245.92 and 1664.73 metric tons of PM_{10} during the February 3 and June 5, 2020, dust event days, respectively. The Road Forks fields discharged 30.16 kg and 50.75 kg of PM_{10} on the February 3 and June 5, 2020, dust event days, respectively. The size of the eroding areas affected the amount of airborne soil loss from different components by controlling the activity of the soil loss components with downwind distance. Accordingly, in the very long fields, the suspension and PM_{10} modes showed greater soil loss, and in the very small fields, the saltation/creep was the dominant component. On June 5, 2020, the North Playa field emitted much greater amounts of wind-eroded soil than during the event of February 3, 2020, due to the higher wind speed on that date. RFP is a smaller field compared to North Playa, and during dust events, it generated a lesser amount of soil loss and PM_{10}. However, due to its position relative to the wind direction and I-10, this field poses a more serious threat to public health and safety. Using the hourly PM_{10} soil loss output from the SWEEP model, NLCD land cover data, emission locations and their geometry, and multiple meteorological data products, the hourly concentrations of PM_{10} over the playa emanating from the selected fields were simulated by the AERMOD modeling system for the two dust event days. The highest hourly concentration of PM_{10} during the dust event of February 3, 2020, was around 130,266 $\mu g/m^3$, 866 times the NAAQS daily concentration limit for PM_{10}. In regard to the convective dust event with higher winds on June 5, 2020, the maximum hourly PM_{10} concentration was estimated to be 217,565 $\mu g/m^3$, and the dominant wind direction was southwesterly. The results from AERMOD simulated PM_{10} dispersions were also verified by blowing dust observations from NMDOT webcam photos and visibility data from meteorological sites on the playa.

Potential Particulate Matter and Metal Exposures

The researchers suggest considering the intersection of the results of the SWEEP-AERMOD modeling with the analyses of bioavailable lead, copper, and zinc in the erodible portion of Lordsburg Playa sediments. Of the metallic

elements analyzed, a federal air quality standard exists only for lead (Pb). The primary and secondary Pb standards are 0.15 $\mu g/m^3$ Pb in total suspended particles (TSP) as a 3-month average. The finding of up to 20 ppm of bioavailable lead in the silt fraction of near-playa sediments (lead concentration in the PM_{10} fraction would be assumed to be higher than that in the overall silt fraction due to the general inverse relationship of metal concentration and soil grain size [Al-Rajhi et al., 1996]), and the values of PM_{10} obtained by SWEEP and AERMOD that could exceed 200,000 $\mu g/m^3$, could lead to exposures of at least 4 $\mu g/m^3$ in bioavailable Pb alone, in the PM_{10} fraction alone, at I-10. Given that concentrations of TSP (i.e., wind-transported particles of all sizes) in the dust will be much higher than the PM_{10} concentrations, while keeping in mind the grain size–metal concentration inverse relationship (Al-Rajhi et al., 1996), the exposure to Pb in the regulated category of TSP along I-10 during Lordsburg Playa dust events may be much higher than the 4 $\mu g/m^3$ of bioavailable Pb estimated in PM_{10}. However, the NAAQS for lead represents a 3-month average; actual exposures to dust for travelers at Lordsburg Playa would be very transient in time, not exceeding several hours in a worst-case scenario for each trip crossing the playa. As a result, total average quarterly exposure to airborne lead to travelers exposed to multiple dust events at Lordsburg Playa is likely to be increased by at most a few hundredths of a microgram per cubic meter in an extreme scenario.

Dust exposures to humans along the playa at I-10 to copper and especially zinc have the potential to be much higher. However, no air quality regulatory standard exists for those elements, and their human health effects from aerosol exposure are less studied than those of lead. Experimental evidence exists for bioavailable Cu as a specific promoter of the generalized respiratory inflammation caused by metal mixtures in airborne particulate matter (Pardo et al., 2015; Palleschi et al., 2018). The high concentration of copper found in at least one sample of Lordsburg Playa silt should be considered a component of potential human health concern in inhaled Lordsburg Playa dust. Inhalation of micron-sized zinc oxide aerosols has been shown to cause respiratory inflammation (Monsé et al., 2021), so a concern over zinc exposure from Lordsburg Playa dust could also be explored (although, since zinc in near-roadway dust is likely derived in large part from tire wear [Councell et al., 2004], which would occur anywhere alongside highways in desert environments, this is not strictly a playa-specific hazard). As with lead, however, exposures to other metals to travelers and highway workers at the playa, although acute, would be short-term and infrequent.

Conclusions, Implications, and Recommendations

Clouds of dust blowing from Lordsburg Playa, a dry lakebed in the Chihuahuan Desert of southwestern New Mexico, represent an acute health and safety hazard to highway traffic on I-10, which crosses the playa. Lordsburg Playa has been reported to be the deadliest stretch of highway in the United States with regard to dust hazard. In addition to the risk of vehicular crashes caused by loss of visibility and/or traction, an additional risk is the exposure to high concentrations of particulate matter and its constituent compounds.

The field investigations highlighted the role of sediment transport and surface crusting in modulating dust emissivity of playa surfaces. Playa sediments generally were rich in wind-erodible silt, composed of minerals common to regional playas, and contained trace to minor amounts of bioavailable metals in those silts, some of which may be derived from vehicle-related emissions settling near the highway. The unlimited supply of coarse sediments along the western playa shoreline, associated with flows of particles entering the playa from slopes above where they were eroded, may contribute to triggering dust events; this zone should be a focus area for dust mitigation efforts, along with beach and delta areas, which also bring sediments into the playa. However, critical friction velocities and dust emissivities were more dependent on surface crust strength, thickness, and disturbance than surface sediment texture.

The actual lakebed surface is not strongly dust emissive when intact and undisturbed, but if crusted playa surfaces become disturbed, dust emission potential is strongly increased. Activities on the playa that degrade the crust and areas with fragile crusts should continue to be restricted. In order to improve highway safety and reduce the risk of

continued dust-related crashes, shutdowns, and particulate matter exposures, the playa should be monitored for and protected against activities that disturb the crust and increase dust emissions. Even a small area of disturbed playa in the wrong place and an unfortunate gust of wind could initiate a dust plume crossing the highway, dangerously reducing visibility and creating a health and safety hazard to those along I-10.

Dust emitted from hotspot fields on the playa both immediately adjacent to the highway and at farther distances can lead to PM_{10} concentrations on the order of or exceeding 100,000 μg/m^3 at I-10, representing associated concentrations of micrograms per cubic meter of bioavailable metals in airborne particles. However, these exposures are likely to be temporally short and not likely to significantly impact the long-term aerosol inhalation burden to anyone caught in a playa dust event. In addition to the existing fixed roadside signage reminding motorists to beware of and drive properly during dust storms, transportation authorities may wish to consider adding advisories to travelers to set vehicular ventilation systems to block intake of outside air during dusty conditions.

This study combined USDA's SWEEP wind erosion model and EPA's AERMOD air dispersion model to quantify dust emission from a playa environment. The field testing and modeling methodologies performed in this study can be adopted to assess the potential intensity of wind erosion and dust emission and identify areas for mitigation at other playas and desert dust hotspots that threaten transportation corridors and infrastructure.

Outputs, Outcomes, and Impacts

Technical Outputs, Outcomes, and Impacts
- PI Thomas Gill was invited to sit as a member of NMDOT's Lordsburg Playa Dust Mitigation Technical Panel.
- PI Thomas Gill was asked to formally evaluate NMDOT's report *Surface Disturbance Analysis of Lordsburg Playa and Adjacent Watersheds*.

Research Outputs, Outcomes, and Impacts
This report has been extracted in part from the contents of these research products.

Peer-Reviewed Publications
- Van Pelt, R.S., Tatarko, J., Gill, T.E., Chang, C., Li, J., Eibedingil, I.G., and Mendez, M., 2020. Dust emission source characterization for visibility hazard assessment on Lordsburg Playa in Southwestern New Mexico, USA. *Geoenvironmental Disasters*, 7(1), 34.
- Eibedingil, I.G., Gill, T.E., Van Pelt, R.S., and Tong, D.Q., 2021. Combining Optical and Radar Satellite Imagery to Investigate the Surface Properties and Evolution of the Lordsburg Playa, New Mexico, USA. *Remote Sensing*, 13, 3402.

Presentations at Conferences, Meetings, and Workshops
- Van Pelt, R.S., Tatarko, J., Chang, C., Rende, W., and Gill, T.E., 2018. Erodibility of and dust emissions from bare soil surfaces in the North American Southwest. Soil and Water Conservation Society Annual Meeting, Albuquerque, New Mexico, August 1, 2018.
- Gill, T.E., 2018. The Dirt On Dust. Science Teachers Association of Texas MiniCAST meeting, El Paso, Texas, October 19, 2018.
- Eibedingil, I.G., 2018. Identification of Surface Endmembers Using Spectral Unmixing in Google Earth Engine. Workshop on Dust Indicators for the National Climate Assessment, George Mason University, Fairfax, Virginia, December 9, 2018.

- Gill, T.E., Lee, J., Kandakji, T., Dominguez, M., Baddock, M., and Eibedingil, I., 2019. 15 Years' Application of Satellite Imagery to Detection and Impact Assessment of Dust Storms in the Southwest USA. NASA Health and Air Quality Applied Science Team (HAQAST) 5th Annual Meeting, Phoenix, Arizona, January 4, 2019.
- Tong, D., Baker, B., Wang, J., Gill, T.E., Eibedingil, I., Van Pelt, S., Lei, H., Liu, Z., Wang, B., Ginoux, P., Pu, B., Huang, M., Kim, D., and Chin, M., 2019. Observing and Forecasting Dust Storms. NASA Health and Air Quality Applied Science Team (HAQAST) 5th Annual Meeting, Phoenix, Arizona, January 4, 2019.
- Tong, D., Baker, B., Wang, J., Gill, T.E., Van Pelt, R.S., Wang, B., Ginoux, P., Pu, B., Lei, H., Liu, Z., and Kim, D., 2019. Rising Dust Storm Activity in the Southwestern United States: Evidence from Long-Term Multiplatform Observations. American Meteorological Society Annual Meeting, Phoenix, Arizona, January 9, 2019.
- Gill, T.E., Dubois, D., Eibedingil, I., Fuentes, J., Jin, L., Li, J., Mendez, M., Tatarko, J., Van Pelt, R.S., and Webb, N., 2019. Assessing the Acute Safety Hazard to Highway Transportation from Blowing Dust at Lordsburg Playa, New Mexico. Transportation, Air Quality, and Health Symposium, Austin, Texas, February 20, 2019.
- Mendez, M., 2019. Site Analysis Using Google Earth Engine: Lordsburg Playa Case Study. Annual Colloquium, Department of Geological Sciences, University of Texas at El Paso, El Paso, Texas, March 7, 2019.
- Gill, T.E., 2019. Characteristics and Implications of Windblown Dust and Sand in the El Paso/Las Cruces Area. New Mexico Dust Conference/New Mexico Department of Environment, Las Cruces, New Mexico, April 17, 2019.
- Eibedingil, I., Mendez, M., and Gill, T.E., 2019. Identification of Land Surface Endmembers of Lordsburg Playa Using Spectral Unmixing in Google Earth Engine. New Mexico Dust Conference/New Mexico Department of Environment, Las Cruces, New Mexico, April 17, 2019.
- Saucedo, J.A., Gill, T., and Jin, L., 2019. In-vitro analysis of particulate matter using simulated lung and gastrointestinal fluids. Doris Duke Conservation Scholars Program Annual Meeting, Chicago, Illinois, April 26, 2019.
- Gill, T.E., Panelist, Workshop on satellite-aided regional dust forecasting for valley fever surveillance, highway accident prevention, and air quality management, New Mexico Department of Health, Santa Fe, New Mexico, August 12, 2019.
- Eibedingil, I.G., Gill, T.E., and Tong, D.Q., 2019. Investigating the Surface Properties and Evolution of a Desert Playa Using Optical and Radar Satellite Imagery Products. American Geophysical Union Annual Meeting, San Francisco, California, December 12, 2019. https://doi.org/10.1002/essoar.10501681.1
- Van Pelt, R.S., Tatarko, J., Gill, T.E., Chang, C., Li, J., Eibedingil, I.G., and Mendez, M., 2019. Dust Source Characterization on Lordsburg Playa in Southwestern New Mexico. American Geophysical Union Annual Meeting, San Francisco, California, December 12, 2019.
- Van Pelt, R.S., Tatarko, J., Gill, T.E., Chang, C., Li, J., Eibedingil, I., and Mendez, M., 2020. Quantitatively Characterizing Dust Source areas at Lordsburg Playa. Ninth National Weather Service Dust Workshop, Coolidge, Arizona, March 3, 2020.
- Gill, T., 2020. Dust Storms: Latest Findings. New Mexico Dust Conference—New Mexico Department of Environment, online, April 6, 2020.
- Gill, T.E., 2020. Characterization of Blowing Dust and Sand Events. Texas Weather Conference—National Weather Service and Texas State Climatologist, online, September 24, 2020.
- Gill, T.E., Tong, D.Q., Sprigg, W., Li, J., Van Pelt, R.S., Ren, L., Bell, J., Chester, Z., Lee, J.A., Eibedingil, I.G., and Kandakji, T., 2021. Using Satellite Data to Support Regional Dust Event Detection and Forecasting in the Southwestern USA—Application to Valley Fever Surveillance, Highway Safety and Air Quality Management. American Meteorological Society Annual Meeting, online, January 12, 2021.

- Li, W.-W., Aguilera, J.A., Soyoung, J., Chavez, M.C., Whigham, L., and Gill, T.E., 2021. Characterization of Exposures and Associated Health Risks in Underserved Near-road Communities due to Traffic Emissions: Recent Investigations in the U.S.-Mexico Border Region. Second Transportation, Air Quality, and Health Symposium, CARTEEH, online, May 18, 2021.
- Gill, T.E., 2021. Dust and Particulate Matter Hazard on I-10 at Lordsburg Playa in Southwestern New Mexico. Second Transportation, Air Quality, and Health Symposium, CARTEEH, online, May 18, 2021.

Technology Transfer Outputs, Outcomes, and Impacts

- Data sets for satellite remote sensing products, spectral unmixing, wind erosion, and air dispersion modeling to characterize surface properties, dust emission, and PM_{10} dispersion at Lordsburg Playa are archived at the CARTEEH data hub and at http://dx.doi.org/10.17632/4pn5vsxxm7.1.
- Data sets for combining optical and radar satellite imagery to investigate the surface properties and evolution of Lordsburg Playa are archived at the CARTEEH data hub and at http://dx.doi.org/10.17632/ds4j2f3765.1.
- Full texts of open-access publications listed above are archived at the CARTEEH data hub.

Education and Workforce Development Outputs, Outcomes, and Impacts

The following students were critical to the success of this research project:

- Julieta Saucedo, undergraduate student, graduated with a B.S. in environmental science from UTEP in May 2020 (shown in Figure 32).

- Marcos Mendez, graduate student, is a candidate for an M.S. in geological sciences at UTEP (shown in Figure 33).

- Iyasu G. Eibedingil, doctoral student, graduated with a Ph.D. in environmental science and engineering at UTEP in May 2021. His dissertation title is Drought, Dust Storm, and Particulate Matter Pollution and Their Interaction at the Cascade of Spatial Scales Across the Western United States (shown in Figure 34).
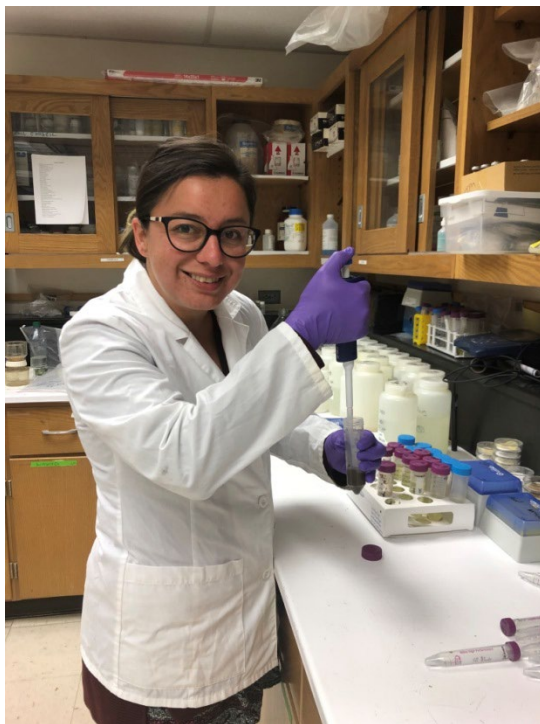
Figure 32. Photo of Julieta Saucedo.

Figure 33. Photo of Marcos Mendez.

Figure 34. Photo of Iyasu G. Eibedingil.

References

Adamiec, E., 2017. Chemical fractionation and mobility of traffic-related elements in road environments. *Environmental Geochemistry and Health*, 39, 1457–1468.

ADOT, 2019. *U.S. 70 Safford to New Mexico State Line Interstate Detour Needs Study*. Report Prepared for the Arizona Department of Transportation, Contract #17–171965, Task #MPD 00018–19, 60 pp.

Allen, B.D., and Lucas, S.G., 2005. Ice age lakes in New Mexico. *New Mexico Museum of Natural History and Science Bulletin*, 28, 107–113.

Al-Rajhi, M.A., Al-Shayeb, S.M., Seaward, M.R.D., and Edwards, H.G.M., 1996. Particle size effect for metal pollution analysis of atmospherically deposited dust. *Atmospheric Environment*, 30, 145–153.

Amer, N.H., and Abbas, A.A., 2015. Combined Influence of Stack Height and Exit Velocity on Dispersion of Pollutants Caused by Helwan Cement Factory (Study using AERMOD Model). *International Journal of Computer Applications*, 121(9), 19–24.

Ashley, W.S., Strader, S., Dziubla, C.C., and Haberlie, A., 2015. Driving blind: weather-related vision hazards and fatal motor vehicle crashes. *Bulletin of the American Meteorological Society*, 96, 755–778.

Associated Press, 2017. 2 killed in freeway crash in NM dust storm. Online at http://www.lcsun-news.com/story/news/local/2017/02/24/2-killed-freeway-crash-nm-duststorm/98369206/, published on February 24, 2017.

Baddock, M.C., Gill, T.E., Bullard, J.E., Dominguez Acosta, M., and Rivera Rivera, N., 2011a. Geomorphology of the Chihuahuan Desert based on potential dust emissions. *Journal of Maps*, 7, 249–259.

Baddock, M.C., Strong, C.L., Murrahy, P.S., and McTainsh, G.H., 2013. Aeolian dust as a transport hazard. *Atmospheric Environment*, 71, 7–14.

Baddock, M.C., Zobeck, T.M., Van Pelt, R.S., and Fredrickson, E.L., 2011b. Dust emissions from undisturbed and disturbed, crusted playa surfaces: cattle trampling effects. *Aeolian Research*, 3, 31–41.

Bhattachan, A., Okin, G.S., Zhang, J., Vimal, S., and Lettenmaier, D.P., 2019. Characterizing the role of wind and dust in traffic accidents in California. *GeoHealth*, 3, 307–328.

Blincoe, L.J., Miller, T.R., Zaloshnja, E., and Lawrence, B.A., 2015. *The economic and societal impact of motor vehicle crashes*. National Highway Traffic Safety Administration Report 812.

Bobo, M., Karl, M.G., Miller, S.W., Spurrier, C., Taylor, J.M., and Toevs, G.R., 2018. AIM-monitoring: a component of the BLM assessment, inventory, and monitoring strategy. U.S. Department of the Interior, Bureau of Land Management, National Operations Center, online at https://doi.org/10.5962/bhl.title.153310

Botkin, T., and Hutchinson, B., 2019. Lordsburg Playa Dust Storm Mitigation Update. Presentation at the USA National Weather Service 8th Dust Storm Workshop, March 2019, Coolidge, Arizona, online at https://www.weather.gov/media/psr/Dust/2019/12_BOTKIN%20DustMitigation_AZ2019.pdf

Botkin, T., and Hutchinson, B., 2020. Lordsburg Playa Dust Storm Mitigation Update. Presentation at the USA National Weather Service 9th Dust Storm Workshop, March 2020, Coolidge, Arizona, online at https://www.weather.gov/media/psr/Dust/2020/9_BOTKIN_DustMitigation_AZ_2020.pdf

Botlaguduru, V.S.V., 2010. *Comparison of AERMOD and ISCST3 models for particulate emissions from ground level sources*. M.S. Thesis, Texas A&M University.

Cahill, T.A., Gill, T.E., Reid, J.S., Gearhart, E.A., and Gillette, D.A., 1996. Saltating particles, playa crusts, and dust aerosols at Owens (dry) Lake, California. *Earth Surface Processes and Landforms*, 21, 621–639.

Chalvatzaki, E., Glytsos, T., and Lazaridis, M., 2015. A methodology for the determination of fugitive dust emissions from landfill sites. *International Journal of Environmental Health Research*, 25, 551–569.

Chavez, M., and Li, W.W., 2020. Comparison of modeled-to-monitored $PM_{2.5}$ exposure concentrations resulting from transportation emissions in a near-road community. *Transportation Research Record*, 24, 130–143.

Cimorelli, A.J., Perry, S.G., Venkatram, A., Weil, J.C., Paine, R.J., and Peters, W.D., 1998. *AERMOD—Description of model formulation*. U.S. Environmental Protection Agency Document EPA-454/R-03-004.

Councell, T.B., Duckenfield, K.U., Landa, E.R., and Callender, E., 2004. Tire-wear particles as a source of zinc to the environment. *Environmental Science and Technology*, 38, 4206–4214.

Cox, D.N., 1973. *Soil survey of Hidalgo County, New Mexico*. U.S. Department of Agriculture Soil Conservation Service.

Davari, M., Khabiri, M.M., and Tafti, M., 2019. The effect of pollutants, dust, and dune sand covered over the surface of asphalt pavements on road safety (case study, Sistan and Balouchestan Province, Iran). *Environmental Studies*, 4, 1123–1129.

Davies, N.M., and Feddah, M.R., 2003. A novel method for assessing dissolution of aerosol inhaler products. *International Journal of Pharmaceutics*, 255, 175–187.

Deetz, K., Klose, M., Kirchnerand, I., and Cubasch, U., 2016. Numerical simulation of a dust event in northeastern Germany with a new dust emission scheme in COSMO-ART. *Atmospheric Environment*, 126, 87–97.

Drexler, J.W., and Brattin, W.J., 2007. An In-Vitro Procedure for Estimation of Lead Relative Bioavailability: With Validation. *Human and Ecological Risk Assessment*, 13, 383–401.

Dust-Quant, 2011. *PI-SWERL User's Guide*; Version 1.3a. DUST-QUANT LLC, Las Vegas, Nevada.

Eibedingil, I.G., Gill, T.E., Van Pelt, R.S., and Tong, D.Q., 2021. Combining Optical and Radar Satellite Imagery to Investigate the Surface Properties and Evolution of the Lordsburg Playa, New Mexico, USA. *Remote Sensing*, 13, 3402.

Etyemezian, V., Gillies, J., Shinoda, M., Nikolich, G., King, J., and Bardis, A., 2014. Accounting for surface roughness on measurements conducted with PI-SWERL: evaluation of a subjective visual approach and a photogrammetric technique. *Aeolian Research*, 13, 35–50.

Etyemezian, V., Nikolich, G., Ahonen, S., Pitchford, M., Sweeney, M., Purcell, R., Gillies, J., and Kuhns, H., 2007. The Portable In-Situ Wind ERosion Laboratory (PI-SWERL): a new method to measure PM_{10} potential for windblown dust properties and emissions. *Atmospheric Environment*, 41, 3789–3796.

Fadavi, A., Abari, M.F., and Nadoushan, M.A., 2016. Evaluation of AERMOD for Distribution Modeling of Particulate Matters (Case Study: Ardestan Cement Factory). *International Journal of Pharmaceutical Research & Allied Sciences*, 5, 262–270.

Federal Highway Administration (FHWA), 2005. *Measuring travel time in freight-significant corridors*. U.S. Department of Transportation, Federal Highway Administration, Office of Freight Management and Operations.

Fick, S.E., Barger, N., Tatarko, J., and Duniway, M., 2019. Induced biological soil crust controls on wind erodibility and dust (PM_{10}) emissions. *Earth Surface Processes and Landforms*, 45, 224–236.

Fubini, B., and Arean, C.O., 1999. Chemical aspects of the toxicity of inhaled mineral dusts. *Chemical Society Reviews*, 28, 373–381.

Gascon, F., Bouzinac, C., Thépaut, O., Jung, M., Francesconi, B., Louis, J., Lonjou, V., Lafrance, B., Massera, S., Gaudel-Vacaresse, A., and Languille, F., 2017. Copernicus Sentinel—2A calibration and products validation status. *Remote Sensing*, 9, 584.

Gill, T.E., 1995. *Dust Generation Resulting from Desiccation of Playa Systems: Studies on Mono and Owens Lakes, California*. Dissertation (Ph.D., Earth Science and Resources), University of California—Davis.

Gill, T.E., Gillette, D.A., Niemeyer, T., and Winn, R.T., 2002. Elemental geochemistry of wind-erodible playa sediments, Owens Lake, California. *Nuclear Instruments and Methods*, B189, 209–213.

Gillette, D., Niemeyer, T.C., and Helm, P.J., 2001. Supply-limited horizontal sand drift at an ephemerally crusted, unvegetated saline playa. *Journal of Geophysical Research—Atmospheres*, 106, 18085–18098.

Goossens, D., and Buck, B., 2009. Dust emission by off-road driving: experiments on 17 arid soil types, Nevada, USA. *Geomorphology*, 107, 118–138.

Goudie, A.S., 2014. Desert dust and human health disorders. *Environment International*, 63, 101–113.

Grigoratos, T., and Martini, G., 2015. Brake wear particle emissions: a review. *Environmental Science and Pollution Research*, 22, 2491–2504.

Haas, T.P., 2017. *Traffic counts—New Mexico interstates*. Report prepared by the New Mexico Department of Transportation for the Transportation Infrastructure Revenue Subcommittee Meeting, October 10, 2017.

Hadlocon, L.S., Zhao, L.Y., Bohrer, G., Kenny, W., Garrity, S.R., Wang, J., Wyslouzil, B., and Upadhyay, J., 2015. Modeling of particulate matter dispersion from a poultry facility using AERMOD. *Journal of the Air and Waste Management Association*, 65(2), 206–217.

Hagen, L.J., Wagner, L.E., Tatarko, J., Skidmore, E.L., Durar, A.A., Steiner, L.J., et al., 1995. Wind erosion prediction system: technical description. Proceedings of WEPP/WEPS Symposium, 9111.

Heckel, P.F., and Lemasters, G.K., 2011. The use of AERMOD air pollution dispersion models to estimate residential ambient concentrations of elemental mercury. *Water, Air, and Soil Pollution*, 219, 377–388.

Hibbs, B., Lee, M., Hawley, J.W., and Kennedy, J.F., 2000. Some notes on the hydrogeology and groundwater quality of the Animas Basin system, southwestern New Mexico. *New Mexico Geological Society Fall Field Conference Guidebook*, 51, 227–234.

Holmes, N.S., and Morawska, L., 2006. A review of dispersion modelling and its application to the dispersion of particles: An overview of different dispersion models available. *Atmospheric Environment*, 40, 5902–5928.

Houser, C.A., and Nickling, W.G., 2001. The emission and vertical flux of particulate matter <10 mum from a disturbed clay-crusted surface. *Sedimentology*, 48(2), 255–267.

Jia, Q., Al-Ansari, N., and Knutsson, S., 2014. Modeling of wind erosion of the Aitik Tailings Dam using SWEEP model. *Engineering*, 6(7), 355–364.

Julien, C., Esperanza, P., Bruno, M., and Alleman, L.Y., 2011. Development of an in vitro method to estimate lung bioaccessibility of metals from atmospheric particles. *Journal of Environmental Monitoring*, 13, 621–630.

Kavouras, I.G., Etyemezian, V., Nikolich, G., Gillies, J., Sweeney, M., Young, M., and Shafer, D., 2009. A new technique for characterizing the efficacy of fugitive dust suppressants. *Journal of the Air and Waste Management Association*, 59, 603–612.

Kayhanian, M., 2012. Trend and concentrations of legacy lead (Pb) in highway runoff. *Environmental Pollution*, 160, 169–177.

Kim, C.S., Anthony, T.L., Goldstein, D., and Rytuba, J.J., 2014. Windborne transport and surface enrichment of arsenic in semi-arid mining regions: examples from the Mojave Desert, California. *Aeolian Research*, 14, 85–96.

King, J., Etyemezian, V., Sweeney, M., Buck, B.J., and Nikolich, G., 2011. Dust emission variability at the Salton Sea, California, USA. *Aeolian Research*, 3, 67–79.

Klose, M., Gill, T.E., Etyemezian, V., Nikolich, G., Zadeh, Z.G., Webb, N.P., and Van Pelt, R.S., 2019. Dust emission from crusted surfaces: insights from field measurements and modelling. *Aeolian Research*, 40, 1–14.

Lader, G., Raman, A., Davis, J.T., and Waters, K., 2016. *Blowing dust and dust storms: one of Arizona's most underrated weather hazards*. NOAA Technical Memorandum NWS-WR-290.

Laity, J., 2003. Aeolian destabilization along the Mojave River, Mojave Desert, California: linkages among fluvial, groundwater, and aeolian systems. *Physical Geography*, 24, 196–221.

Langston, G., and McKenna Neuman, C., 2005. An experimental study on the susceptibility of crusted surfaces to wind erosion: A comparison of the strength properties of biotic and salt crusts. *Geomorphology*, 72, 40–53.

Laskey, S.G., 1938. Geology and Ore Deposits of the Lordsburg Mining District, Hidalgo County, New Mexico. *U.S. Geological Survey Bulletin*, 885.

Lee, J.A., Gill, T.E., Mulligan, K.R., Dominguez Acosta, M., and Perez, A.E., 2009. Land use/land cover and point sources of the 15 December 2003 dust storm in southwestern North America. *Geomorphology*, 105, 18–27.

Li, J., Kandakji, T., Lee, J.A., Tatarko, J., Blackwell, J., Gill, T.E., and Collins, J.D., 2018. Blowing dust and highway safety in the southwestern United States: characteristics of dust emission "hotspots" and management implications. *Science of the Total Environment*, 621, 1023–1032.

Li, J., Lee, J.A., and Gill, T.E., 2017. *Identifying Dust Emission "Hot Spots" in the Southern Plains Region of New Mexico, Oklahoma, and Texas: Effect of Blowing Dust on Highway*. Southern Plains Transportation Center Report No. SPTC14.1-39-F, 46 pp.

Li, J., Okin, G.S., Herrick, J.E., Belnap, J., Munson, S.M., and Miller, M.E., 2010. A simple method to estimate threshold friction velocity of wind erosion in the field. *Geophysical Research Letters*, 37, L10402.

Macpherson, T., Nickling, W.G., Gillies, J.A., and Etyemezian, V., 2008. Dust emissions from undisturbed and disturbed supply-limited desert surfaces. *Journal of Geophysical Research—Earth Surface*, 113(F2), F02S04.

Malvern Instruments Ltd., 2007. *Mastersizer 2000 user manual*. Worcestershire, United Kingdom: Malvern Instruments.

Martin, R., 2018. In vitro assessment of arsenic mobility in historical mine waste dust using simulated lung fluid. *Environmental Geochemistry and Health*, 40, 1037–1049.

Maurer, T., and Gerke, H.H., 2011. Modelling aeolian sediment transport during initial soil development on an artificial catchment using WEPS and aerial images. *Soil and Tillage Research*, 117, 148–162.

McKenna Neuman, C., and Maxwell, C., 2002. Temporal aspects of the abrasion of microphytic crusts under grain impact. *Earth Surface Processes and Landforms*, 27(8), 891–908.

McKenna Neuman, C., Maxwell, C., and Rutledge, C., 2005. Spatial and temporal analysis of crust deterioration under particle impact. *Journal of Arid Environments*, 60(2), 321–342.

McLemore, V.T., and Elston, W.E., 2000. Geology and mineral occurrences of the mineral districts of Hidalgo County, southern New Mexico. *New Mexico Geological Society Annual Fall Field Conference Guidebook*, 51, 253–262.

Middleton, N.J., 2017. Desert dust hazards: a global review. *Aeolian Research*, 24, 53–63.

Mitroo, D., Gill, T.E., Pratt, K.A., and Gaston, C.J., 2019. $ClNO_2$ production from N_2O_5 uptake on saline dusts: new insights into potential inland sources of $ClNO_2$. *Environmental Science and Technology*, 53, 7442–7452.

Monsé, C., Raulf, M., Jettkant, B., Van Kampen, V., Kendzia, B., Schürmeyer, L., Seifert, C.E., Marek, E.M., Westphal, G., Rosenkranz, N., and Merget R., 2021. Health effects after inhalation of micro- and nano-sized zinc oxide particles in human volunteers. *Archives of Toxicology*, 95, 53–65.

Morman, S.A., and Plumlee, G.S., 2013. The role of airborne mineral dusts in human disease. *Aeolian Research*, 9, 203–212.

New Mexico Climate Center, 2019. Online at https://weather.nmsu.edu/nmdot-lp/, retrieved November 1, 2020.

New Mexico Department of Transportation, 2018. Dust Mitigation Safety Projects: Interstate 10. Presentation at the New Mexico Transportation and Construction Conference. April 2018, Las Cruces, New Mexico.

Nicoll, K., Hahnenberger, M., and Goldstein, H.L., 2020. "Dust in the wind" from source-to-sink: analysis of the 14–15 April 2015 storm in Utah. *Aeolian Research*, 46, 100532.

Novlan, D.J., Hardiman, M., and Gill, T.E., 2007, A synoptic climatology of blowing dust events in El Paso, Texas, from 1932–2005. *Preprints, 16th Conference on Applied Climatology*, American Meteorological Society, J3.12.

Ono, D., Kiddoo, P., Howard, C., Davis, G., and Richmond, K., 2011. Application of a Combined Measurement and Modeling Method to Quantify Windblown Dust Emissions from the Exposed Playa at Mono Lake, California. *Journal of the Air and Waste Management Association*, 61, 1036–1045.

Palleschi, S., Rossi, B., Armiento, G., Montereali, M.R., Nardi, E., Tagliani, S.M., Inglessis, M., Gianfagna, A., and Silvestroni, L., 2018. Toxicity of the readily leachable fraction of urban $PM_{2.5}$ to human lung epithelial cells: Role of soluble metals. *Chemosphere*, 196, 35–44.

Pan, J., Zhao, H., Wang, Y., and Liu, G., 2021. The Influence of Aeolian Sand on the Anti-Skid Characteristics of Asphalt Pavement. *Materials*, 14, 5523.

Pardo, M., Shafer, M.M., Rudich, A., Schauer, J.J., and Rudich, Y., 2015. Single exposure to near roadway particulate matter leads to confined inflammatory and defense responses: possible role of metals. *Environmental Science and Technology*, 49, 8777–8785.

Pauley, P.M., Baker, N.L., and Barker, E.H., 1996. An observational study of the "Interstate 5" dust storm case. *Bulletin of the American Meteorological Society*, 77, 693–720.

Pi, H., Sharratt, B., Feng, G., Lei, J., Li, X., and Zheng, Z., 2016. Validation of SWEEP for creep, saltation, and suspension in a desert-oasis ecotone. *Aeolian Research*, 20, 157–168.

Pimentel, D., Harvey, C., Resosudarmo, P., Sinclair, K., Kurz, D., McNair, M., Crist, S., Shpritz, L., Fitton, L., Saffouri, R., and Blair, R., 1995. Environmental and economic costs of soil erosion and conservation benefits. *Science*, 267, 1117–1123.

Prospero, J.M., Ginoux, P., Torres, O., Nicholson, S.E., and Gill, T.E., 2002. Environmental characterization of global sources of atmospheric dust identified with the Nimbus-7 Total ozone mapping spectrometer (TOMS) absorbing aerosol products. *Reviews of Geophysics*, 40, 1002.

Pye, K., and Tsoar, H., 2009. *Aeolian sand and sand dunes*. Springer, Berlin, 476 pp.

Reheis, M.C., Budahn, J.R., and Lamothe, P.J., 2002. Geochemical evidence for diversity of dust sources in the southwestern United States. *Geochimica et Cosmochimica Acta*, 66, 1569–1587.

Reynolds, R.L., Yount, J.C., Reheis, M., Goldstein, H., Chavez, P., Fulton, R., Whitney, J., Fuller, C., and Forester, R.M., 2007. Dust emission from wet and dry playa surfaces in the Mojave Desert, USA. *Earth Surface Processes and Landforms*, 32, 1811–1827.

Rivera Rivera, N.R., Gill, T.E., Bleiweiss, M.P., and Hand, J.L., 2010. Source characteristics of hazardous Chihuahuan Desert dust outbreaks. *Atmospheric Environment*, 44, 2457–2468.

Rood, A.S., 2014. Performance evaluation of AERMOD, CALPUFF, and legacy air dispersion models using the Winter Validation Tracer Study dataset. *Atmospheric Environment*, 89, 707–720.

Smolders, E., and Degryse, F., 2002. Fate and effect of zinc from tire debris in soil. *Environmental Science and Technology*, 36, 3706–3710.

Soil Survey Staff, 2019. Soil Survey Geographic (SSURGO) Database for Lordsburg Playa, New Mexico. Online at https://websoilsurvey.sc.egov.usda.gov/App/WebSoilSurvey.aspx, retrieved October 1, 2020.

Sperazza, M., Moore, J.N., and Hendrix, M.S., 2004. High-resolution particle size analysis of naturally occurring very fine-grained sediment through laser diffractometry. *Journal of Sedimentary Research*, 74, 736–743.

Sweeney, M., Etyemezian, V., Macpherston, T., Nickling, W., Gillies, J., Nikolich, G., and McDonald, E., 2008. Comparison of PI-SWERL with dust emission measurements from straight-line wind tunnel. *Journal of Geophysical Research*, 113, F01012.

Sweeney, M.R., Zlotnik, V.A., Joeckel, R.M., and Stout, J.E., 2016. Geomorphic and hydrologic controls of dust emissions during drought from Yellow Lake playa, West Texas, USA. *Journal of Arid Environments*, 133, 37–46.

Tartakovsky, D., Stern, E., and Broday, D.M., 2016. Dispersion of TSP and PM_{10} emissions from quarries in complex terrain. *Science of the Total Environment*, 542, 946–954.

Tatarko, J., Van Donk, S.J., Ascough, J.C., and Walker, D.G., 2016. Application of the WEPS and SWEEP models to non-agricultural disturbed lands. *Heliyon*, 2, e00215.

Tian, S., Liang, T., and Li, K., 2019. Fine road dust contamination in a mining area presents a likely air pollution hotspot and threat to human health. *Environment International*, 128, 201–209.

Tong, D., Feng, I., Wang, G., and Gill, T., 2021. Rising Dust and Impact on American Public: How Many People Were Killed by Windblown Dust Events? Presented at the Air and Waste Management Association 114th Annual Conference and Exhibition, Virtual Conference, June 11–14, 2021.

U.S. Department of the Interior, Bureau of Land Management, 1998. Emergency closure of the Lordsburg playa to off-highway vehicles (OHV), Hidalgo County, NM. *Federal Register*, 63(122), 34661.

U.S. Department of the Interior, Bureau of Land Management, 2018. *Road Forks Dust Mitigation Project Environmental Assessment*. Document No. IT4RM-L000-2018-0056-EA. Online at https://dot.state.nm.us/content/dam/nmdot/D1/I-10%20Dust%20Mitigation%20Project%20Road%20Forks.pdf

U.S. Department of Transportation, 2006. 5.1.4 Recommended Guidelines—FHWA. Online at https://mutcd.fhwa.dot.gov/rpt/tcstoll/chapter514.htm, retrieved November 4, 2020.

U.S. EPA, 2010. Air Quality Models | TTN—Support Center for Regulatory Atmospheric Modeling | U.S. EPA. Online at https://www.epa.gov/scram/air-quality-dispersionmodeling

U.S. EPA, 2015. *AERMINUTE User's Guide*. Research Triangle Park, NC, Office of Air Quality Planning and Standards.

U.S. EPA, 2018a. AERMOD Model Formulation and Evaluation. Online at https://www3.epa.gov/ttn/scram/models/aermod/aermod_mfed.pdf

U.S. EPA, 2018b. *User's Guide for the AERMOD Terrain Preprocessor (AERMAP)*. Research Triangle Park, NC, Office of Air Quality Planning and Standards.

U.S. EPA, 2019. *User's guide for the AERMOD Meteorological Preprocessor (AERMET)*. Research Triangle Park, NC, Office of Air Quality Planning and Standards.

U.S. EPA, 2020. *User's Guide for AERSURFACE Tool*. Research Triangle Park, NC, Office of Air Quality Planning and Standards.

USDA-ARS, 2007. *Single-event Wind Erosion Evaluation Program SWEEP User Manual Draft*.

USDA-NRCS, 2019. Web Soil Survey. Online at https://websoilsurvey.sc.egov.usda.gov/App/WebSoilSurvey.aspx, retrieved on March 27, 2020.

Van Pelt, R.S., Baddock, M.C., Zobeck, T.M., D'Odorico, P., Ravi, S., and Bhattachan, A., 2017. Total vertical sediment flux and PM_{10} emissions from disturbed Chihuahuan Desert surfaces. *Geoderma*, 293, 19–25.

Van Pelt, R.S., Tatarko, J., Gill, T.E., Chang, C., Li, J., Eibedingil, I.G., and Mendez, M., 2020. Dust emission source characterization for visibility hazard assessment on Lordsburg Playa in Southwestern New Mexico, USA. *Geoenvironmental Disasters*, 7(1), 34.

Von Holdt, J.R.C., Eckard, F.D., Baddock, M.C., and Wiggs, G.F.S., 2019. Assessing landscape dust emission potential using combined ground-based measurements and remote sensing data. *Journal of Geophysical Research*, 124, 1080–1098.

Westbrook, J.A., and Sullivan, P.S., 2006. Fugitive dust modeling with AERMOD for PM_{10} emissions from a municipal waste landfill. Proceedings of the A&WMA Specialty Conference, Guideline on Air Quality Models: Applications and FLAG Developments 2006, Air and Waste Management Publication, CP-164, 207–223.

Wickham, J., Homer, C., Vogelmann, J., McKerrow, A., Mueller, R., Herold, N., and Coulston, J., 2014. The Multi-Resolution Land Characteristics (MRLC) Consortium—20 Years of Development and Integration of USA National Land Cover Data. *Remote Sensing*, 6, 7424–7441.

Willis, G.E., and Deardorff, J.W., 1981. A laboratory study of dispersion from a source in the middle of the convectively mixed layer. *Atmospheric Environment*, 15, 109–117.

Wiseman, C.L.S., 2014. Characterizing metal(loid) solubility in airborne PM_{10}, $PM_{2.5}$, and PM_1 in Frankfurt, Germany, using simulated lung fluids. *Atmospheric Environment*, 89, 282–289.

Wiseman, C.L.S., 2015. Analytical methods for assessing metal bioaccessibility in airborne particulate matter: A scoping review. *Analytica Chimica Acta*, 877, 9–18.

World Health Organization, 2018. *Global status report on road safety 2018*. World Health Organization, Geneva.

Wragg, J., 2011. An inter-laboratory trial of the unified BARGE bioaccessibility method for arsenic, cadmium, and lead in soil. *Science of the Total Environment*, 409, 4016–4030.

Yang, L., Jin, S., Danielson, P., Homer, C., Gass, L., Bender, S.M., Case, A., Costello, C., Dewitz, J., Fry, J., and Funk, M., 2018. A new generation of the United States National Land Cover Database: Requirements, research priorities, design, and implementation strategies. *ISPRS Journal of Photogrammetry and Remote Sensing*, 146, 108–123.

Zheng-chao, H.U., 2018. The wind-blown sand hazard potential evaluation of highway on dry up lake-basin region of Taitema Lake. *Territory Natural Resources Study*, 2, 13.

Zobeck, T.M., and Van Pelt, R.S., 2006. Wind-induced dust generation and transport mechanics on a bare agricultural field. *Journal of Hazardous Materials*, 132, 26–38.

Zou, B., Zhan, F.B., Wilson, J.G., and Zeng, Y., 2010. Performance of AERMOD at different time scales. *Simulation Modelling Practice and Theory*, 18, 612–623.